UMS
UNIVERSITI MALAYSIA SABAH

BORNEO SCIENCE

The Journal of Science and Technology

ONLINE ISSN : 2231-9085 | ISSN : 1394- 4339

BORNEO SCIENCE

A JOURNAL OF SCIENCE AND TECHNOLOGY

BORNEO SCIENCE is a journal of science and technology published twice a year. It publishes original articles on all aspects of research in science and technology of general or regional interest particularly related to Borneo. Manuscripts submitted must not have been published, accepted for publication, or be under consideration elsewhere. Borneo Science welcomes all categories of papers: full research papers, short communications, papers describing novel methods, review papers and book reviews. Views expressed in the articles do not represent those of the Editorial Board and the University.

BORNEO *SCIENCE* *merupakan jurnal sains dan teknologi yang diterbitkan dwitahunan. Jurnal ini menerbitkan artikel asli dalam kesemua bidang sains dan teknologi secara umum mahupun dalam kepentingan serantau, terutamanya yang berkaitan dengan Borneo. Manuskrip yang dihantar bukan yang telah diterbitkan, telah diterima untuk diterbitkan, atau sedang dipertimbangkan untuk diterbitkan. Borneo Science mengalu-alukan semua jenis kertas kerja sama ada hasil penyelidikan, komunikasi pendek, penjelasan suatu kaedah, ulasan kertas kerja atau ulasan buku. Pandangan yang ditulis dalam artikel Borneo Science tidak menggambarkan pendapat Sidang Editor dan Universiti.*

DOI: https://doi.org/10.51200/bsj.v42i1

BORNEO SCIENCE

A JOURNAL OF SCIENCE AND TECHNOLOGY

BORNEO SCIENCE

A JOURNAL OF SCIENCE AND TECHNOLOGY

ONLINE ISSN 2231-9085 | ISSN 1394-4339

BORNEO SCIENCE

A JOURNAL OF SCIENCE AND TECHNOLOGY
JURNAL SAINS DAN TELNOLOGI

Volume 42 Issue 1

March 2021

CONTENT
KANDUNGAN

Page
Muka
Surat

ORIGINAL ARTICLES

BorneoScience
The Journal of Science & Technology
Volume 42 Issue 1 : March 2021
Online ISSN : 2231-9085 | ISSN : 1394-4339

DYNAMIC SIMULATION ON THE RECOVERY OF 2-ACETYL PYRROLINE (2-AP) IN A PACKED BED COLUMN USING RICE HUSK CHAR AS SOLID ADSORBENT

Carla Goncalves De Olievera Sarmento[1], Mohd Hardyianto Vai Bahrun[1,], Jidon Janaun[1], Awang Bono[2,*], Duduku Krishnaiah[3]**

[1]Chemical Engineering Programme, Faculty of Engineering, Universiti Malaysia Sabah, Jalan UMS, 88400 Kota Kinabalu, Sabah, Malaysia
[2]GRISM Innovative Solutions, Kota Kinabalu, Sabah, Malaysia
[3]Department of Chemical Engineering, Anurag University, Hyderabad, Telangana 500088, India

*Corresponding author. E-mail: awangbono@gmail.com : hardyvai14@gmail.com

Received 11th Nov 2020; accepted 25th July 2021
Available online 12 August 2021
DOI:

ABSTRACT. *Fragrant rice is known to contain the aromatic compound of 2-Acetyl Pyrroline (2-AP). This compound has been known as a major compound that gives fragrant characteristics in rice. However, this compound is volatile and easily escapes from the rice upon the drying process. In order to recover the release of 2-AP from rice upon drying, a packed bed adsorption system is employed using treated agricultural waste as a solid adsorbent. The experimental adsorption study in a batch mode for 2-AP onto treated rice husk char (TRHC) was used as a case study for this present work. Influences of three operational parameters towards the dynamic adsorption of 2-AP onto TRHC in a packed bed column were investigated by measuring the breakthrough and saturation time and mass transfer zone. This study suggests the possibility of treated agricultural waste as an alternative to capture the lost 2-AP during the paddy drying process.*

KEYWORDS. Adsorption; Aromatic rice; Breakthrough curve; Treated rice husk; Simulation

INTRODUCTION

Rice is the most important food in Asia, and is regarded as a staple food for Asian. Aroma is among the important qualities of rice that is responsible for the pleasant smell in rice. The characteristic that gives fragrance to rice is the compound known as 2-acetyl pyrroline (2-AP), with a chemical formula of C_6H_9NO (Hien et al., 2006). 2-AP is a highly volatile aromatic compound in rice; thus, it escapes easily together with moisture contained in the rice during the paddy drying process and during storage, thus making the rapid aroma evaporation highly disadvantageous to the aroma sensory quality of the rice (Baradi & Elepano, 2012). In addition, Yoshihashi et al. (2005) reported that the 2-AP compound in the aromatic rice is present in low concentration, making it easier to lose through diffusion from the rice to the environment. Other than that, storage at high temperature has an effect on the concentration 2-AP in the rice and causes it to decrease (Kongkiattikajorn, 2008). The consequence of the aroma loss in the rice is the loss of profit annually for the global rice production. Therefore, this has prompted numerous advancements in upstream and downstream processes to increase the yield of paddy production while maintaining or improving the sensory quality of the aromatic rice. One of the methods to capture the loss 2-AP during the paddy drying process is the adsorption process. Adsorption method involves the transference of solute from the bulk fluid to the adsorbent's surfaces.

A packed bed column is widely used in practical applications for adsorption in continuous dynamic operation because of its simple operation method for industrial application (Hanafy et al., 2019). Packed bed adsorption column is a device that is filled with a specific adsorbent that adheres to a specific solute adsorbate when passing through the adsorbent bed (Bahrun et al., 2021). Several commercial simulators are available and can solve sets of complex algebraic, partial and ordinary equations of packed bed adsorption columns, and one of them is Aspen Adsorption V11 developed by AspenTech. Aspen Adsorption is a comprehensive flowsheeting simulator tool for adsorption process with and without reaction (AspenONE, 2009).

This present work seeks to investigate the dynamic behavior of treated rice husk char (TRHC) adsorbent for recovering volatile aromatic compound, 2-Acetyl Pyrroline (2-AP) conducted in a packed bed column. The numerical simulation was conducted using Aspen Adsorption V11 simulation package, by solving the governed mathematical model describing a packed bed adsorption column. The dynamic behaviours of TRHC for 2-AP recovery were investigated from the breakthrough curve performance at different operational conditions including inlet flow rate, inlet concentration and bed column height. The performance was measured in terms of time and mass transfer zone.

MATERIALS AND METHODS

2.1. THE ORETICAL ASSUMPTIONS OF SIMULATIONS

The following general assumptions were considered for simulation in a packed bed column:

a) The behavior of the fluid is assumed as a plug flow
b) A linear driving force (LDF) model is used to represent the transmigration between solid-fluid phases
c) A lumped mass transfer equation is used with solid-film resistance. The lumped mass transfer equation consists of external film resistance and intraparticle surface resistance
d) The equilibrium adsorption is sufficiently described using Langmuir equation
e) The isotherm constants of 2-AP on TRHC in aqueous-phase is assumed to be similar as in gas-phase

2.2. GOVERNING MATHEMATICAL MODEL OF A PACKED BED COLUMN

The ideal plug-flow mathematical model describing the adsorption process in a packed bed column is expressed as in Equation 1 (AspenONE, 2009).

$$v_i \frac{\partial C_i}{\partial z} + \varepsilon \frac{\partial C_i}{\partial t} + \rho_s \frac{\partial Q_i}{\partial t} = 0 \quad (1)$$

where ρ_s is the bulk solid density (kg/m^3), ε is the bed voidage (m^3 void/m^3 bed), v_i is the superficial velocity (m/s) of component *i*, C_i is the gas-phase concentration (mg/L) of component *i*, and Q_i is the solid-phase loading (mg/g) of component *i*.

The terms $\partial Q/\partial t$ can be well-represented by a simplified kinetic model, known as linear driving force (LDF) approximation. The LDF model assumed the mass transfer driving force is a linear function of the solid phase loading. Equation 2 shows the LDF model equation (Glueckauf, 1955).

$$\frac{\partial Q_i}{\partial t} = k_{LDF}(Q_i^* - Q_i) \quad (2)$$

where k_{LDF} is the lumped mass transfer coefficient (1/s). In this work, two independent mass transfer diffusions were lumped by linear addition into the LDF mass transfer coefficient (Bono, 1989).

$$\frac{1}{k_{LDF}} = \frac{R_p}{3(1-\varepsilon)k_f} + \frac{{R_p}^2}{15D_s} \quad (3)$$

For the range of $0.0055 < Re_p < 55$ found in this work, the film mass transfer coefficient, k_f (m/s) can be calculated using Sherwood, *Sh* correlation

$$Sh = \frac{2R_p k_f}{D_m} = \frac{1.09}{\varepsilon} Sc^{0.33} Re^{0.33} \quad (4)$$

where R_p is TRHC adsorbent particle radius (m), D_m is the molecular diffusivity (m^2/s), and *Sh*, *Re* and *Sc* are Sherwood, Reynolds and Schmidt dimensionless numbers, respectively. The molecular diffusivity of 2-AP in air, D_m can be calculated using Fuller equation as expressed in Equation 5 (Coker, 2007; Fuller et al., 1966).

$$D_m = \frac{10^{-3} T^{1.75} \left(\frac{1}{M_A} + \frac{1}{M_B}\right)^{\frac{1}{2}}}{P\left[(\sum V_A)^{\frac{1}{3}} + (\sum V_B)^{\frac{1}{3}}\right]^2} \quad (5)$$

where T is temperature (K), P is pressure (atm), M_A and M_B are molecular weights of 2-AP and air, and V_A and V_B are molar volumes of 2-AP and air, respectively. For the determination of intraparticle surface diffusion, D_s (cm^2/s), the correlation developed by Suzuki & Kawazoe (1975) for volatile organic compounds is used as a preliminary value for model input, as expressed in Equation 6.

$$D_s = 1.1 \times 10^{-4} e^{\left(\frac{-5.32 T_b}{T}\right)} \quad (6)$$

where T_b is the boiling point of 2-AP adsorbate (K), and T is the adsorption temperature (K). The intraparticle surface diffusion, D_s values obtained for this study were in the range of 10^{-7} cm^2/s, which is in agreement with the range reported for gaseous-phase surface diffusivity (Green & Perry, 2008).

2.3. DATA EXTRACTION FOR CASE STUDY

This current work was based on the experimental data by Sarmento (2021), and it was used as a case study for this simulation. The dynamic adsorption simulation was conducted by using Aspen Adsorption V11. The required data for the simulation on the adsorbent properties and adsorption isotherm are presented in Table 1 and Table 2, respectively.

Table 1: Some physical properties of treated rice husk char (TRHC) adsorbent

Parameter	Value
TRHC adsorbent particle diameter, mm	1.00
Bulk density, kg/m^3	455
Bulk porosity (m^3 void/m^3 bed)	0.35

Table 2: The Langmuir adsorption isotherm constant for 2-AP onto treated rice husk char (TRHC) (Sarmento, 2021)

Langmuir isotherm	Q_{max} (mg/g)	625
	b (L/mg)	0.00146
	R^2	0.9925

2.4. PARAMETRIC STUDIES ON PACKED BED COLUMN PROCESS PARAMETERS

Various operating process parameters were conducted to investigate the performance of the packed bed adsorption column at various operating conditions by evaluating the breakthrough curve profile. The varying parameters included inlet 2-AP flow rate, inlet 2-AP concentration, and bed column height while keeping the bed column diameter at 1.5 m. The base case concentration used in this work (0.0610 ppm) was assumed to follow the concentration of a commercialized Basmathi rice as taken from Nadaf et al. (2006). The parametric studies were conducted by changing around the original base value, as described in Table 3.

Table 3: Parametric studies with their respective varying parameters value

Simulation no.	Inlet flow rate, Q (kmol/s)	Inlet concentration, C_0 (ppm)	Bed column height, H (m)
1	3.8879×10^{-7}	0.0610	2.0
2	4.8599×10^{-7}		
3	5.8319×10^{-7}		
4	4.8599×10^{-7}	0.0488	2.0
5		0.0610	
6		0.0732	
7	4.8599×10^{-7}	0.0610	1.6
8			2.0
9			2.4

2.5. DYNAMIC ADSORPTION PERFORMANCE ANALYSIS

The results from the converged numerical iteration are presented in both data tables and graphical presentation. Three key indexes are used to describe the performance of the dynamic adsorption in a packed bed column. There are breakthrough time (t_b), saturation time (t_s), and length of mass transfer zone (L_{MTZ}). The breakthrough time, t_b is taken when the C/C0 reached 0.05, while the saturation time, ts is taken when the C/C_0 reached 0.95. The length of the mass transfer zone, L_{MTZ} is calculated following Equation 7.

$$L_{MTZ} = H\left(1 - \frac{t_b}{t_s}\right) \quad (7)$$

RESULTS AND DISCUSSION

Once all the required input parameters and physical properties have been determined, the mathematical model framework could be solved by numerical solution built in the software. Three parameters' effects on the bed column performance were investigated to evaluate the dynamic behavior of the system when certain operational parameters change. The three parameters include inlet flow rate, inlet concentration, and bed column height. The bed column performance was measured by assessing the breakthrough time (t_b), saturation time (t_s), as well as the length of the mass transfer zone (L_{MTZ}).

3.1. INFLUENCE OF INLET 2-ACETYL PYRROLINE FLOWRATE ON BREAKTHROUGH CURVE

A strong influence of the inlet 2-AP flowrate on the breakthrough and saturation time was observed in Figure 1(a). The inlet flow rates were varied at 3.8879×10^{-7}, 4.8599×10^{-7}, and 5.8319×10^{-7} kmol/s, while keeping constant the 2-AP concentration at 0.061 ppm and TRHC column height at 2.0 m. At the increasing inlet 2-AP flow rate, the breakthrough time and saturation time decrease. This is due to the insufficient contact time between 2-AP molecules with the TRHC adsorbent bed, thus making the 2-AP molecules to have limited reach towards the active sites of the adsorbent (Ahmed et al., 2020). In terms of the breakthrough shape and gradient, the higher the flow rate, the broader the gradient of the breakthrough curve, as reported in Table 4. Broaden breakthrough curve indicated by the higher L_{MTZ}. Changes in the gradient of the curves indicated that changing inlet 2AP flow rate affects the mass transfer resistance (da Rosa et al., 2015). The details on the breakthrough time, saturation time and length of mass transfer zone at different inlet flow rate are summarized in Table 4.

Table 4: Parametric studies - dependence on inlet 2-AP flow rate

Flowrate (kmol/s)	t_b (hour)	t_s (hour)	L_{MTZ} (m)
3.8879×10^{-7}	74.55	112.34	0.6729
4.8599×10^{-7}	59.54	89.79	0.6738
5.8319×10^{-7}	49.54	74.76	0.6747

3.2. INFLUENCE OF INLET 2-ACETYL PYRROLINE CONCENTRATION ON BREAKTHROUGH CURVE

The effect of inlet 2-AP concentration on the breakthrough curve was investigated by varying the inlet 2-AP concentration while keeping the same inlet flow rate of 4.8599×10^{-7} kmol/s and bed height of 2.0 m. The concentrations under study were 0.0488, 0.0610 and 0.0732 ppm. The breakthrough curves at different inlet 2-AP concentrations were illustrated in Figure 1(b). It was observed that increasing inlet 2-AP concentration caused earlier breakthrough and saturation time.

Apart from that, it was noted in Figure 1(b) that the influence of inlet 2AP concentration does not much affect the breakthrough and saturation time. A change in ±20% inlet 2-AP concentration only caused the breakthrough and saturation time to change by approximately 2%. This, by means of changing the concentration by ±20%, is relatively small compared to the amount of adsorbent present in the bed column that is readily available for adsorption sites. Though small changes were observed when initial 2-AP concentration changed, it is worth noting that increasing inlet 2-AP concentration leads to a steeper breakthrough curve, as indicated by a lower L_{MTZ} at a higher inlet 2-AP concentration in Table 5. This is because a larger concentration gradient is provided at higher inlet concentration, which enhances the mass transfer rates in both fluid and solid phases (da Rosa et al., 2015). The details on the breakthrough time, saturation time and length of mass transfer zone on different inlet concentrations are tabulated in Table 5.

Table 5: Parametric studies - dependence on inlet 2-AP concentration

Concentration (ppm)	t_b (hour)	t_s (hour)	L_{MTZ} (m)
0.0488	60.42	91.33	0.6770
0.0610	59.54	89.79	0.6739
0.0732	58.84	88.57	0.6713

3.3. INFLUENCE OF BED COLUMN HEIGHT ON BREAKTHROUGH CURVE

The analysis of the influence of TRHC column height on the breakthrough curve performance is presented in Figure 1(c). The bed column heights investigated were 1.6 m, 2.0 m, and 2.4 m, while keeping inlet flow rate and concentration constant at 4.8599×10^{-7} kmol/s and 0.0610 ppm, respectively.

The breakthrough curve in Figure 1(c) indicates that the breakthrough time of the TRHC column increases from 47.54 hours to 71.55 hours as the TRHC bed column height increases from 1.6 m to 2.4 m. A longer bed column height means a large amount of TRHC in the column bed. Consequently, it provides a large surface area available for adsorption binding sites leading to an increase in the breakthrough time. Moreover, longer bed column height enhances the gas-solid contact time in the column, eventually causing a deep transport of 2-AP onto TRHC adsorbent (Hymavathi & Prabhakar, 2019; Tan et al., 2020). In terms of the gradient of the curve, longer bed column height causes the length of the mass transfer zone to increase, as stated in Table 6. A reasonable explanation for this is most probably due to abundant mass transfer zones at higher bed column height, and thus less rapid transference of adsorbate to the adsorption sites (Jangde et al., 2019). The details on the breakthrough time, saturation time, and length of mass transfer zone at different bed column height were presented in Table 6.

Table 6: Parametric studies - dependence on bed column height

Bed column height (m)	t_b (hour)	t_s (hour)	L_{MTZ} (m)
1.6	47.54	71.75	0.5400
2.0	59.54	89.79	0.6738
2.4	71.55	107.83	0.8076

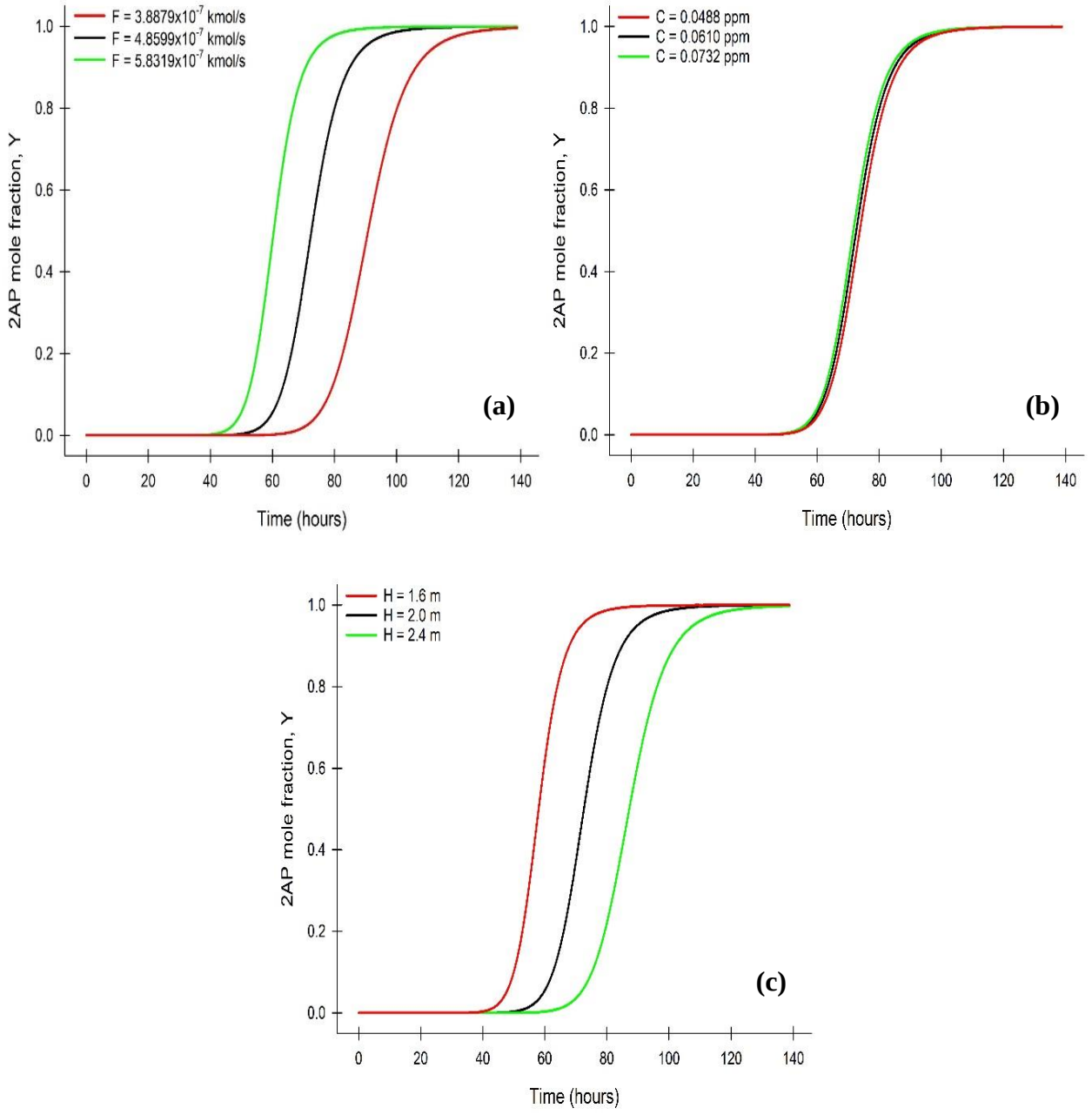

Figure SEQ Figure * ARABIC 1: Effect of (a) inlet flowrate [C_0=0.0610 ppm, H=2.0 m]; (b) inlet concentration [F=4.8599×10^{-7} kmol/s, H=2.0 m]; (c) bed column height [F=4.8599×10^{-7} kmol/s, C_0=0.0610 ppm] on the breakthrough curve

CONCLUSION

This present work seeks to investigate the dynamic adsorption of a volatile aromatic compound, 2-Acetyl Pyrroline (2-AP), onto treated rice husk char (TRHC) in a packed bed column. The investigations were conducted through numerical computation using Aspen Adsorption V11, using data from the batch experimental study and some reliable predictions using available correlations. Based on this present study, some conclusions could be drawn:

1. An alternative in using treated agricultural waste (TRHC) to recover volatile compound (2-AP) gives promising results through dynamic simulation;
2. The packed bed column filled with treated rice husk char with column height and diameter of 2.0 m and 1.5 m, with inlet 2-AP flow rate and concentration of 4.8599×10^{-7} kmol/s and 0.0610 ppm, respectively able to capture volatile 2-AP with 89.79 hours operation time, so that the user just needs to replace the whole packed bed column in every 89.79 hours or 3.74 days;
3. The influence of inlet 2-AP flow rate and concentration are inversely proportional to the saturation (operation) time of the system;
4. On the other hand, the influence of TRHC bed column height is directly proportional to the system's operation time.

However, further investigation needs to be executed to establish and verify the assumption of similar adsorption constants for 2-AP onto TRHC in aqueous and gas phases.

ACKNOWLEDGMENT

The authors want to acknowledge the financial support given by the Ministry of Higher Education Malaysia, under Fundamental Research Grant Scheme number FRGS0417/TK2015.

REFERENCES

Ahmed, S., Unar, I. N., Khan, H. A., Maitlo, G., Mahar, R. B., Jatoi, A. S., Memon, A. Q., & Shah, A. K. (2020). Experimental study and dynamic simulation of melanoidin adsorption from distillery effluent. *Environmental Science and Pollution Research*, *27*(9), 9619–9636.

AspenONE. (2009). *AspenONE v7.3 Reference Guide*. AspenTech Inc.

Bahrun, M. H. V., Kamin, Z., Anisuzzaman, S. M., & Bono, A. (2021). Assessment of Adsorbent for Removing Lead (Pb) Ion in an Industrial-Scaled Packed Bed Column. *Journal of Engineering Science and Technology*, *16*(2), 1213–1231.

Baradi, M. A. U., & Elepano, A. R. (2012). Aroma Loss in Rice as Affected by Various Conditions during Postharvest Operations. *Philippine Agricultural Scientist*, *95*(3), 260–266.

Bono, A. (1989). *Sorptive Separation of Simple Water Soluble Organics* (Doctoral dissertations, University of Surrey, Guildford, United Kingdom). Retrieved from https://openresearch.surrey.ac.uk/esploro/outputs/doctoral/Sorptive-Separation-of-Simple-Water-Soluble-Organics/99511759402346#files_and_links

Coker, A. K. (2007). *Ludwig's Applied Process Design for Chemical and Petrochemical Plants* (4th ed.). Gulf Professional Publishing. da Rosa, C. A., Ostroski, I. C., Gimenes Meneguin, J., Gimenes, M. L., & Barros, M. A. S. D. (2015). Study of Pb2+ adsorption in a packed bed column of bentonite using CFD. *Applied Clay Science*, *104*, 48–58.

Fuller, E. N., Schettler, P. D., & Giddings, J. C. (1966). A new method for prediction of binary gas-phase diffusion coefficients. *Industrial and Engineering Chemistry*, *58*(5), 18–27. https://doi.org/10.1021/ie50677a007

Glueckauf, E. (1955). Theory of chromatography. Part 10: Formulae for diffusion into spheres and their application to chromatography. *Transactions of the Faraday Society*, *51*, 1540–1551.

Green, D. W., & Perry, R. H. (2008). *Perry's Chemical Engineers' Handbook* (8th ed). The McGraw-Hill Companies, Inc.

Hanafy, H., Sellaoui, L., Thue, P. S., Lima, E. C., Dotto, G. L., Alharbi, T., Belmabrouk, H., Bonilla-Petriciolet, A., & Lamine, A. Ben. (2019). Statistical physics modeling and interpretation of the adsorption of dye remazol black B on natural and carbonized biomasses. *Journal of Molecular Liquids*, *299*, 112099.

Hien, N. L., Yoshihashi, T., Sarhadi, W. A., & Hirata, Y. (2006). Sensory Test for Aroma and Quantitative Analysis of 2-Acetyl-1-Pyrroline in Asian Aromatic Rice Varieties. *Plant Production Science*, *9*(3), 294–297. https://doi.org/10.1626/pps.9.294

Hymavathi, D., & Prabhakar, G. (2019). Modeling of cobalt and lead adsorption by Ficus benghalenesis L. in a fixed bed column. *Chemical Engineering Communications*, *206*(10), 1264–1272.

Jangde, V., Umathe, P., Antony, P. S., Shinde, V., & Pakade, Y. (2019). Fixed-bed column dynamics of xanthate-modified apple pomace for removal of Pb(II). *International Journal of Environmental Science and Technology*, *16*(10), 6347–6356.

Kongkiattikajorn, J. (2008). Effect of Storage Time and Temperature on Volatile Aroma Compounds and Physicochemical Properties of Rice. *Kasetsart Journal - Natural Science*, *42*, 111–117.

Nadaf, A. B., Krishnan, S., & Wakte, K. V. (2006). Histochemical and biochemical analysis of major aroma compound (2-acetyl-1-pyrroline) in basmati and other scented rice (Oryza sativa L.). *Current Science*, *91*(11), 1533–1536.

Sarmento, C. G. D. O. (2021). *Adsorption of 2-Acetyl-1-Pyrroline (2-AP) by Using Rice Husk Chars* (Unpublished master's thesis). Universiti Malaysia Sabah, Sabah, Malaysia.

Suzuki, M., & Kawazoe, K. (1975). Effective Surface Diffusion Coefficients of Volatile Organics on Activated Carbon during Adsorption from Aqueous Solution. *Journal of Chemical Engineering of Japan*, *8*(5), 379–382. https://doi.org/10.1252/jcej.8.379

Tan, W.-H., Bahrun, M. H. V., Surugau, N., & Bono, A. (2020). Evaluation of Adsorption Dynamic Retention of Copper Ion in Porous Agricultural Soil. *Transactions on Science and Technology, 7*(3), 90–100.

Yoshihashi, T., Huong, N. T. T., Surojanametakul, V., Tungtrakul, P., & Varanyanond, W. (2005). Effect of Storage Conditions on 2-Acetyl-1-pyrroline Content in Aromatic Rice Variety, Khao Dawk Mali 105. *Journal of Food Science*, *70*(1). https://doi.org/10.1111/j.1365-2621.2005.tb09061.x

BorneoScience
The Journal of Science & Technology
Volume 42 Issue 1 : March 2021
Online ISSN : 2231-9085 | ISSN : 1394-4339

EFFECTS OF CRITICAL MICELLE CONCENTRATION OF ANIONIC SURFACTANTS AND THEIR TOXICITY TO AQUATIC ORGANISMS

Siti Afida, I*; Noorazah, Z and Razmah, G

[1]Advanced Oleochemical Technology Division (AOTD), Malaysian Palm Oil Board, 6, Persiaran Institusi, Bandar Baru Bangi, 43000 Kajang, Selangor, Malaysia

*Correspomdimg author. Email: siti.afida@mpob.gov.my

Received 3rd May 2020; accepted 24th July 2021.
Available online 12 August 2021
DOI: https://doi.org/10.51200/bsj.v42i1

ABSTRACT. *The critical micelle concentration (CMC) is the concentration of surfactants above which micelles are formed. The effects of CMC of methyl ester sulfonates (MES) on ecotoxicological behaviour of freshwater organisms in predicting the risk levels contributed from the surfactant used were determined. The surface tension of palm-based MES with various carbon chain lengths (C_{12}, C_{14} and C_{16}) was measured to determine the CMC. Ecotoxicity tests were conducted on three different aquatic organisms: green algae (Raphidocelis subcapitata), freshwater crustacean (Daphnia magna) and freshwater fish (Tilapia nilotica). The effective concentration of MES that caused 50% fish mortality (LC_{50}), crustacean immobilization (EC_{50}) and algae inhibition (EC_{50}) was determined. Through surface tension analyses, the CMC obtained for MES C_{12}, C_{14} and C_{16} was 1000 mg/L, 900 mg/L and 12 mg/L, respectively. The LC_{50} of MES C_{12}, C_{14} and C_{16} were 391 mg/L, 22.6 mg/L and 12.6 mg/L, respectively, in fish. The crustacean EC_{50} of MES C_{12}, C_{14} and C_{16} were >100 mg/L, 77.6 mg/L, and 1.15 mg/L. Meanwhile, algae EC_{50} of MES C_{12}, C_{14} and C_{16} was 541 mg/L, 399 mg/L and >10 mg/L, respectively. Relative comparison showed that D. magna was observed to be more sensitive compared to R. subcapitata and T. nilotica towards MES of the same chain length. A linear relationship was observed between CMC and ecotoxicity values. The lower the CMC value, the lower is the LC_{50} or EC_{50} value and the surfactant becomes more toxic. It is suggested that the CMC value can be used as a toxicity indicator for anionic surfactant by considering that the EC_{50} value of a surfactant will be reached before its CMC value.*

KEYWORDS: CMC, Ecotoxicity, Aquatic organisms, Environment

INTRODUCTION

The anionic surfactants are best known for their wide use which contributed about 60% of the world surfactant production. Excessive use of any type of surfactant and their disposal in the environment, especially in an aquatic environment, could seriously affect the ecosystems, hence should be monitored and regulated (Ivanković and Hrenović, 2010). Many aquatic toxicity studies toward surfactants have been conducted due to the public concerns (Fernández-Serrano *et al*., 2014; Jurado *et al*., 2012b; Ríos *et al*., 2017; Jurado *et al*., 2012a). The ecotoxicity of different commercial surfactants (six anionics, two amphoteric and one nonionic) towards planktonic freshwater green algae and

marine diatoms have also been studied by Pavlic *et al*., (2005) whereby all of these commercial surfactants caused toxic effects on freshwater green algae and marine diatoms.

The toxicity of surfactants in an aquatic environment is affected by their chemical properties. The study by Calamari and Marchetti (1973) reported the increase in toxicity of surfactants with increasing cellular permeability of aquatic species in response to the surface tension reduction. The toxicity value of a surfactant has also been correlated with its critical micelle concentration (CMC). The CMC is a concentration of surfactant at which it forms micelles. The study conducted by Hisano and Oya (2010) revealed the reduction of ecotoxicity of sodium linear alkylbenzene sulfonate (LAS) sample as the CMC of this surfactant increased.

Methyl ester sulphonate (MES) is an anionic surfactant derived from sulphonation of palm-based fatty acid methyl esters. It is used as the active ingredient in laundry detergent due to its performance such as excellent detergency and less sensitivity to water hardness. The global market of fatty methyl ester sulfonates (FMES) is expected to reach USD 2.49 billion by 2025 according to Grand View Research due to consumers' awareness on cleanliness and environmental-friendly issues (Market Research Store, 2015b). The major manufactures of MES are Stepan Company (United States of America), Lion Corporation (Japan), Jiangsu Haiqing Biotechnology (China), Huish Detergents (United States of America), Guangzhou Lonkey Industrial Co Ltd (China), and KL-Kepong Oleomas (Malaysia) (Market Research Store, 2015a). This paper aims to determine the effects of CMC of MES on aquatic toxicity in predicting the risk levels contributed by the surfactant used.

MATERIALS AND METHODS

Test substances

Palm-based MES with various carbon chain lengths (C_{12}, C_{14} and C_{16}) were produced from palm stearin methyl esters at the Malaysian Palm Oil Board (MPOB). Potassium dichromate, $K_2Cr_2O_7$ 99.9% AR Grade, from Friendemann Schmidt, Germany, was used as the reference compound.

Surface tension measurement

The CMC values were determined by measuring the surface tension of different concentrations of surfactant solutions at test temperature (25 ºC) using a tensiometer model Tensiometer K100 (Kruss GmbH, Germany) equipped with a 2 cm platinum plate. The stock solution of MES (500 mg/L) was prepared by diluting the surfactant in deionized water. From the stock solution, a series of MES solutions (at different concentrations) were prepared. The platinum plate was cleaned and heated to a reddish orange colour with a Bunsen burner before use. A graph of surface tension value against MES concentration was plotted. The concentration at which discontinuous change in slope occurs is defined as the CMC.

Aquatic toxicity of surfactant

The aquatic toxicity of MES was tested using three different test organisms namely green algae (*Raphidocelis subcapitata*), freshwater crustacean (*Daphnia magna*) and freshwater fish (*Tilapia nilotica*). The method used for ecotoxicity test using fish and freshwater crustacean were according

to the test guideline OECD 203, Fish acute toxicity test and OECD 202, *Daphnia* sp., acute immobilisation test, respectively. Both methods were well described by Razmah *et al*. (2015).

The procedures for ecotoxicity test using freshwater algae were briefly described according to test guideline OECD 201, Algae growth inhibition test (Siti Afida *et al*., 2017). The green algae, *R. subcapitata* (ATCC® 22662™) obtained from the American Type Culture Collection (Maryland, USA) was used as the test species. Five concentrations were prepared for each MES sample with a separation factor not exceeding 3.2, *i.e*. 0 mg/L, 62 mg/L, 197 mg/L, 627 mg/L and 2000 mg/L. These test solutions were exposed to exponentially-growing cultures of *R. subcapitata* and incubated in an incubator (EYELA FLI-2000, Japan,) at 25ºC, 14 hours light cycle (4000 Lux) and 10 hours dark cycle, and shook at 100 rpm. After 72 hours of exposure, the number of algae cells was measured using a particle counter (Beckman Counter Z2, USA). The average growth rate of algae was calculated using the following formula:

$$\mu_{i-j} = \frac{\ln X_j - \ln X_i}{t_j - t_i} \ (\text{day}^{-1}) \ .$$

where:
μ_{i-j} is the average specific growth rate from time i to j;
X_i is the biomass at time *i*;
X_j is the biomass at time *j*
t is the period of test

Meanwhile, the percent inhibition of algae growth rate was calculated using the following formula:

$$\%I_r = \frac{\mu_C - \mu_T}{\mu_C} \times 100$$

where:
$\%I_r$ is the percent inhibition in average specific growth rate;
μ_C is the mean value for average specific growth rate (μ) in the control group;
μ_T is the average specific growth rate for the treatment replicate.

Calculation of effective concentration (EC_{50})

The EC_{50} (effective concentration at 50% algae growth inhibition) values of the samples were determined from the plot of percentage of growth rate inhibition against concentration. All calculations were tabulated using Microsoft Excel.

The respective LC_{50} (lethal concentration which kills 50% of the *T. nilotica*) and EC_{50} (concentration which immobilizes 50% of the *D. magna* after exposure) values for toxicity tests of fish and freshwater crustaceans were calculated via probit analysis with 95% confidence limits using Statistical Package for the Social Sciences (SPSS) software.

RESULTS AND DISCUSSION

Critical micelle concentration (CMC) of methyl ester sulfonates (MES) homologues

The surface tensions of MES were determined and plotted against concentrations to obtain CMC values. The surface tension plots for MES C_{12}, MES C_{14} and MES C_{16} are presented in Fig. 1, 2 and 3, respectively. The CMC value refers to the concentration at which discontinuous change in surface tension slope occurs. The surfactant‘s monomers assemble to form a closed aggregate (micelle) in which the hydrophobic tails are shielded from water while the hydrophilic heads face the water at CMC.

The MES exhibited an approximately linear decrease in surface tension followed by a plateau. The CMC values of MES C_{12}, C_{14}, and C_{16} obtained were 1000 mg/L, 900 mg/L, and 12 mg/L, respectively. The CMC is correlated with the number of hydrophobic tails of MES. The MES becomes less polar and less soluble in water with a higher number of hydrophobic tails. MES C_{12} had the highest CMC value and was more soluble in water compared to MES C_{14} and MES C_{16}. It can be concluded that as the chain length of MES increases, the CMC value of MES decreases.

Sanchez leal *et al*. (1991) also reported an excellent linear relationship between the CMC value and molecular weight of anionic surfactant. Becher *et al*. (1984) established an equation to relate CMC with the number of carbons and ethoxy groups. The CMC increases with a decrease in the partial charge of the head groups, indicating an increase in solubility of the surfactant molecule as the charge is more widely distributed throughout the molecule. As the carbon chain length of MES increases, the micelles are formed at lower concentrations and are less soluble in water.

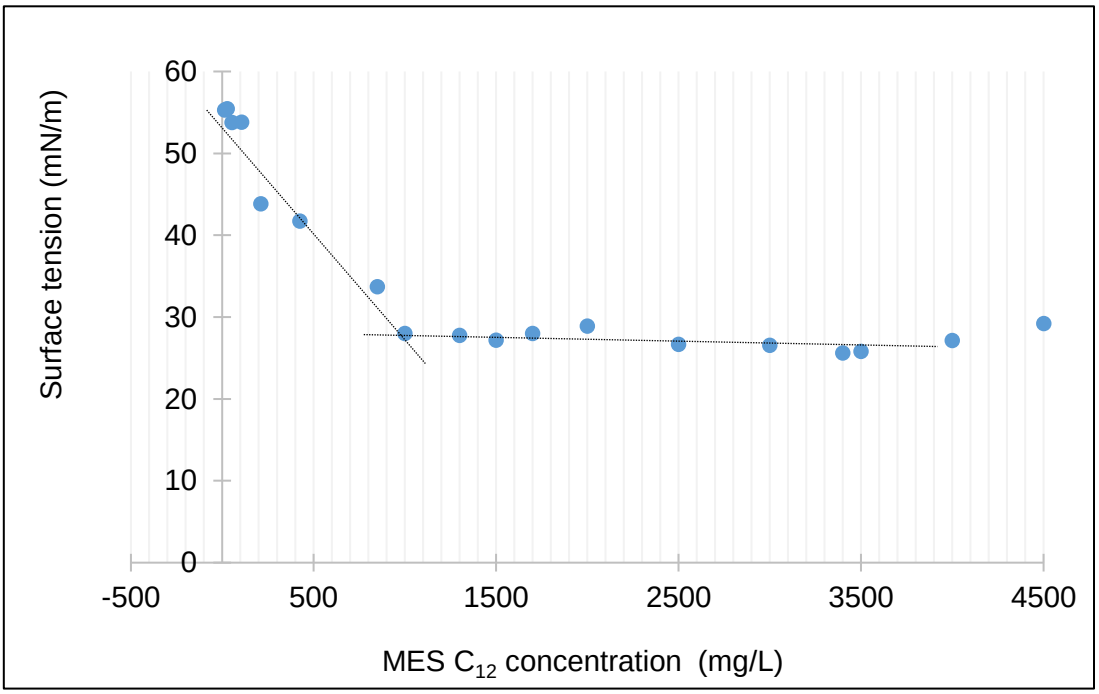

Figure 1: Critical micelle concentration (CMC) for methyl ester sulfonates (MES) C_{12}

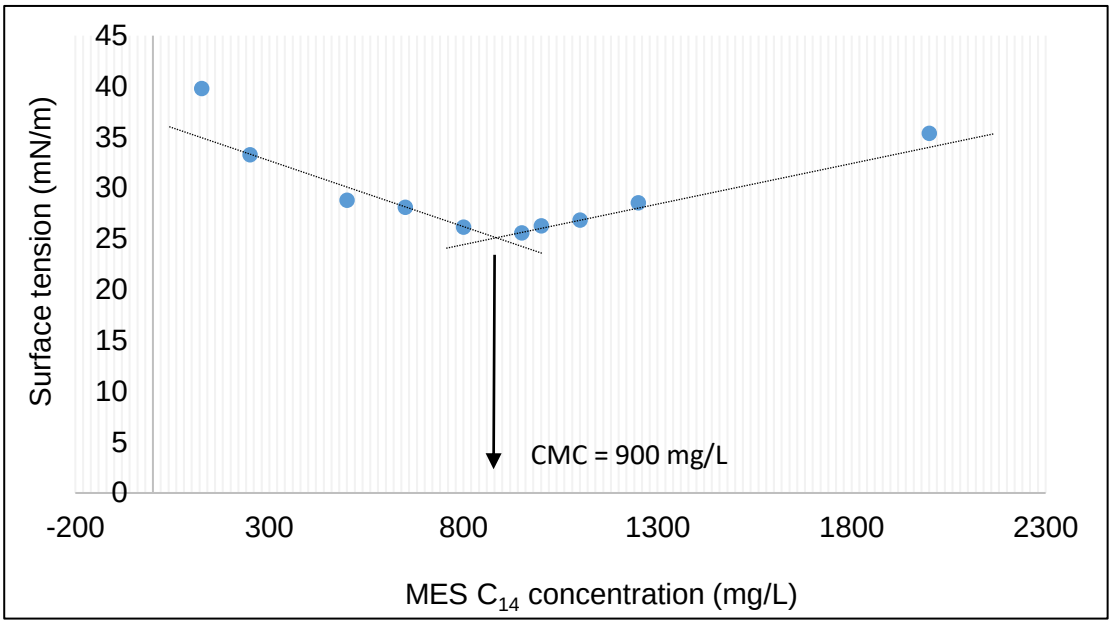

Figure 2: Critical micelle concentration (CMC) for methyl ester sulfonates (MES) C_{14}

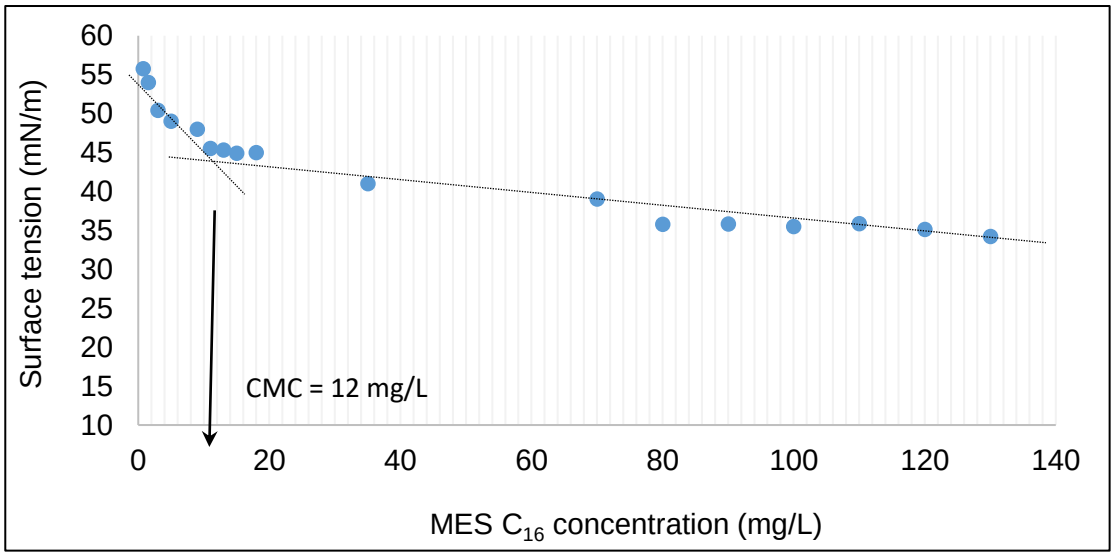

Figure 3: Critical micelle concentration (CMC) for methyl ester sulfonates (MES) C_{16}

Ecotoxicity of methyl ester sulfonates (MES) homologues towards *Raphidocelis subcapitata, Daphnia magna* and *Tilapia nilotica*

Individual toxicity values for different chain lengths of MES are shown in Table 1. The LC_{50} of MES C_{12}, C_{14} and C_{16} was 391 mg/L, 22.6 mg/L and 12.6 mg/L, respectively, in fish. The crustacean EC_{50} for MES C_{12}, C_{14} and C_{16} was >100 mg/L, 77.6 mg/L and 1.15 mg/L, respectively. Meanwhile, the algae EC_{50} of MES C_{12}, C_{14} and C_{16} was 541 mg/L, 399 mg/L and >10 mg/L, respectively.

The toxic effects of MES with the same chain length were higher towards *D. magna* compared to *T. nilotica* and *R. subcapitata*. The *R. subcapitata* was less sensitive towards the MES. According to Razmah *et al*. (2015), *D. magna* was more sensitive to the ecotoxicity effects of MES compared to *T. nilotica*.

MES C12, the shortest carbon chain length, was least toxic among other MES chain lengths with a toxicity range from 100 mg/L to 541 mg/L. The toxicity values of MES increased as the number of carbon chain lengths increases. MES C12 can be classified as practically non-toxic according to GESAMP (2014) since the EC_{50} value is higher than 100mg/L.

Table 1: Acute ecotoxicity of MES towards *Raphidocelis subcapitata, Daphnia magna and Tilapia nilotica*

Test Organisms	MES C_{12}	MES C_{14}	MES C_{16}
Raphidocelis subcapitata (EC_{50}, mg/L)	541	399	>10
Daphnia magna * (EC_{50}, mg/L)	>100	77.6	1.15
Tilapia nilotica * (LC_{50}, mg/L)	391	22.6	12.6

* Data published by Razmah *et al.* (2015)

The aquatic toxicity for anionic surfactants such as MES depends mainly on the length of the carbon chain of the molecule. The toxicity level of a substance correlates with the chain length of the alkyl group (Toshiharu *et al*., 2006). This correlation has also been observed in the homologues of alcohol sulphates and alkylbenzene sulphonates in which the longer the carbon chain, the more toxic the anionic surfactant (Fendinger, 1994; Protokor, 1992). The possible reason for toxicity increase with homologue chain length might be due to greater interaction of the heavier homologues with cell membranes (Ivankovic and Hrenovic, 2010). However, a systematic dependence of the toxicity on the chain length is only recognizable in fully water-soluble compounds (Garcia *et al*., 2001). The ecotoxicity trend of MES was also reported by Razmah *et al*. (2016) by which MES of shorter carbon chains were less toxic than MES with longer carbon chains. Nevertheless, this palm-based MES are not expected to cause any environmental concerns on aquatic organisms due to their rapid biodegradation properties in the environment and only 10%–30% of MES are used in detergent products (Razmah *et al*., 2016).

The effects of CMC and ecotoxicity towards several test organisms are shown in Fig. 4. It can be seen that CMC is clearly related to toxicity as the substances are more toxic with lower CMC values, depending on the organisms assayed.

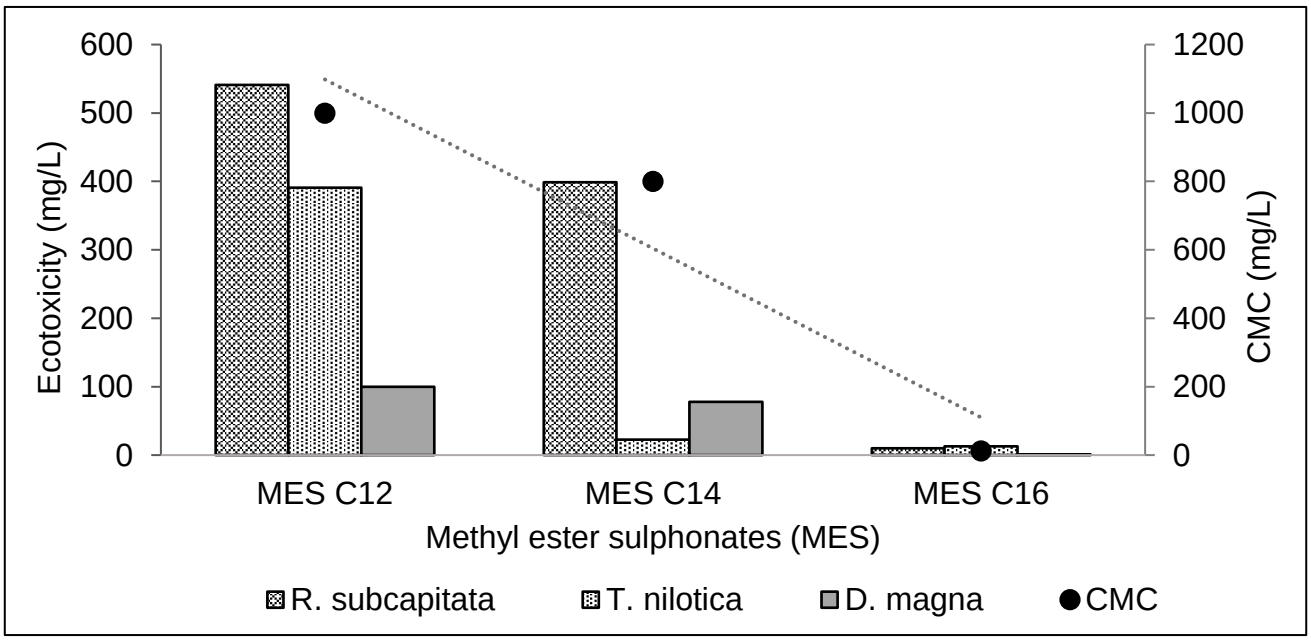

Figure 4: The effects of CMC and ecotoxicity towards *Raphidocelis subcapitata, Daphnia magna,* and *Tilapia nilotica.*

Fernández-Serrano *et al*. (2014) reported that when the CMC of anionic surfactant or mixtures increased, the toxicity of anionic surfactant towards three different organisms (*Vibrio fischeri, Daphnia magna,* and microalgae) decreased. Meanwhile, Inacio *et al*., (2011) reported that the toxic effects of surfactant depended on its hydrophilic head groups, whereby the toxicity level was significantly lower in polar surfactants than the non-polar surfactants. This observation is related to the penetration of surfactant into phospholipids of the organism's cellular membrane. In terms of surfactant, the longer the length of the alkyl chain, the higher the hydrophobicity, which then allows the surfactant to penetrate and interact with the membrane phospholipids. The interaction between surfactant and cell membranes can destabilise and/or destruct the organism's cell membranes and increase the toxicity level of a surfactant (Fernández-Serrano' *et al*., 2014; Inácio *et al*., 2011).

CONCLUSION

In conclusion, the CMC of MES decreased with the increase in chain length of MES. Similarly, the ecotoxicity of MES increased with the increase in chain length of MES. The toxic effects of MES with the same chain length were higher towards *D. magna* compared to *T. nilotica* and *R. subcapitata*. There is a strong relationship between the CMC and ecotoxicity values of MES surfactant, whereby the CMC value decreases as the ecotoxicity of MES increases. The CMC value can be used as a toxicity indicator for anionic surfactant by considering that the EC_{50} value of a surfactant will be reached before its CMC value.

ACKNOWLEDGMENT

The authors would like to thank the Director-General of Malaysian Palm Oil Board (MPOB) for the permission to publish this paper. Special thanks are also extended to members of the Environmental and Product Assessment (EPA) Unit of Advanced Oleochemical Technology Division (AOTD) for their technical assistance and support.

REFERENCES

Becher, P., (1984). Hydrophile−lipophile balance: history and recent developments (Langmuir lecture, 1983). J. Dispersion Sci. Technol *5:* 81–96.

Calamari, D.; Marchetti, R., (1973). The toxicity of mixture of metals and surfactants to rainbow trout (*Salmo gairdneri rich*.). Water Research, 7: 1453-1464.

Fendinger, N. J., (1994) Environmental behaviour and fate of anionic surfactants. Environmental Chemistry of Lakes and Reservoirs (Baker, L A ed.). American Chemical Society, Washington, p. 528-557.

Fernández-Serrano, M.; Jurado, E.; Fernández-Arteaga, A.; Ríos, F.; Lechuga, M., (2014). Ecotoxicological assessment of mixtures of ether carboxylic derivative and amine-oxide-based non-ionic surfactants on the aquatic environment. Journal of Surfactants and Detergents, 17: 1161-1168.

Garcia, M. T.; Ribosa, I.; Guindulain, T.; Sanchez-Leal, J.; Vives-Rego, J., (2001). Fate and effect of monoalkyl quaternary ammonium surfactants in the aquatic environment. Environ. Pollut, 111: 169-75.

GESAMP, (2014). *Revised GESAMP Hazard Evaluation Procedure for Chemical Substances Carried by Ships*, International Maritime Organization.

Hisano, N.; Oya, M., (2010). Effects of surface activity on aquatic toxicity of binary surface mixtures. Journal of oleo science, 59: 589-599.

Inácio, Â. S.; Mesquita, K. A.; Baptista, M.; Ramalho-Santos, J.; Vaz, W. L.; Vieira, O. V., (2011). In vitro surfactant structure-toxicity relationships: Implications for surfactant use in sexually transmitted infection prophylaxis and contraception. PLoS One, 6:19850.

Ivanković, T.; Hrenović, J., (2010). Surfactants in the environment. *Archives of* Industrial Hygiene and Toxicology, 61: 95-110.

Jurado, E.; Fernández-Serrano, M.; Lechuga, M.; Ríos, F., (2012a). Environmental impact of ether carboxylic derivative surfactants. Journal of Surfactants and Detergents, 15: 1-7.

Jurado, E.; Fernández-Serrano, M.; Olea, J. N.; Lechuga, M.; Jiménez, J.; Ríos, F., (2012b). Acute toxicity of alkylpolyglucosides to Vibrio fischeri, Daphnia magna and microalgae: a comparative study. Bulletin of environmental contamination and toxicology, 88: 290-295.

Market Research Store (2015b). *Global Fatty Methyl Ester Sulfonates (FMES) Market is expected to Reach USD 1.58 Billion in 2020* [Online]. Available: http://www.marketresearchstore.com/news/global-fatty-methyl-ester-sulfonates-fmes-market-is-45 [Accessed 15/8/2015

Market Research Store, (2015a). Global Fatty Methyl Ester Sulfonates (FMES) Market for Household Detergents, Personal Care Products and Other Applications, 2014 - 2020.

Pavlić, Ž.; Vidaković-Cifrek, Ž.; Puntarić, D., (2005). Toxicity of surfactants to green microalgae *Pseudokirchneriella subcapitata* and *Scenedesmus subspicatus* and to marine diatoms *Phaeodactylum tricornutum* and *Skeletonema costatum*. Chemosphere, 61: 1061-1068.

Potokor, M. S., (1992). Acute, subacute and chronic toxicity data on anionics. Anionic Surfactants, Biochemistry, Dermatology (Gloxhuber, C and Kunstler, K eds.). 2nd ed., Surfactant Science Series, 43: 81-116.

Razmah, G.; Siti Afida, I.; Noorazah, Z.; Hazimah, A. H.; (2016). Acute ecotoxicity (48-hr EC_{50}) assessment of palm-based methyl ester sulphonates (MES) towards *Daphnia magna*. Journal of Oil Palm Research, 28: 74-80.

Razmah, G.; Siti Afida, I.; Zulina, A.M.; Noorazah, Z.; Hazimah, A.H., (2015). A comparative study of the ecotoxicity of palm-based methyl ester sulphonates (MES) to *Tilapia* and *Daphnia magna*. Journal of Oil Palm Research, 28: 387-392.

Ríos, F.; Lechuga, M.; Fernández-Serrano, M.; Fernández-Arteaga, A., (2017). Aerobic biodegradation of amphoteric amine-oxide-based surfactants: Effect of molecular structure, initial surfactant concentration and pH. Chemosphere, 171: 324-331.

Sanchez Leal, J.; González, J. J.; Comelles, F.; Campos, E.; Ciganda, T., (1991). Biodegradability and Toxicity of anionic surfactant. Acta hydrochim hydrobiol, 19: 703-709.

Siti Afida, I.; Razmah, G.; Zulina, A.M.; Noorazah, Z., (2017). Ecotoxicology Study of Various Homologues of Methyl Ester Sulfonates (MES) Derived from Palm Oil. Journal of Surfactants and Detergents, 20: 1467–1473.

Toshiharu, T.; Horoshi, O.; Kazuaki, M.; Yutaka, T., (2006). Ecotoxicity of Tetradecanoic Acid, 2-sulfo-, 1-methylester, Sodium Salt (C14MES). Journal of Oleo Science, 55: 121-126.

BorneoScience
The Journal of Science & Technology
Volume 42 Issue 2 : March 2021
Online ISSN : 2231-9085 | ISSN : 1394-4339

AN IMAGE ENHANCEMENT METHOD BASED ON A S-SHARP FUNCTION AND PIXEL NEIGHBORHOOD INFORMATION

Libao Yang, Suzelawati Zenian*, Rozaimi Zakaria

Faculty of Science and Natural Resources, Universiti Malaysia Sabah,
88400 Kota Kinabalu, Sabah, Malaysia.

** Corresponding author: Suzelawati Zenian*
Email: suzela@ums.edu.my

Received 26th March 2020; accepted 8th July 2021.
Available online 12 August 2021
DOI: https://doi.org/10.51200/bsj.v42i1.4463

ABSTRACT. *Image enhancement is a significant field in image processing. This paper proposes an image enhancement method based on an S-sharp function of grayscale transformation and neighborhood information. Firstly, a function is established based on the sine function. Then, the image threshold is added into the function. Finally, the result grayscales are modified by parameter* b_{ij}*, where parameter* b_{ij} *is determined by the image pixel neighborhood information. In general, in the result image, each pixel grayscale is determined by both the sine function with threshold and the parameter* b_{ij}*. In the experiment results, the* ***NIEM*** *method (we proposed) achieves better performance than the comparison algorithms. It gets the smallest MSE and the highest PSNR, SSIM. In image Lena test, MSE value:330.8151, PSNR value:22.9350, and SSIM value: 0.9451. In image Pout test, MSE value:132.0988, PSNR value:26.9218, and SSIM value: 0.9604.*

KEYWORDS. Image enhancement, S-sharp function, Standard deviation, Threshold.

INTRODUCTION

Image enhancement is an important field in image processing. The purpose of image enhancement is to improve the visual effect of the input image and turn the fuzzy image into a clear image, thus laying a solid foundation for the subsequent image analysis and image understanding. Image enhancement methods may be categorized into two broad classes: transform domain methods and spatial domain methods. The techniques in the first category are based on modifying the frequency transform of an image. However, computing a two-dimensional transform for a large array (image) is a very time-consuming task even with fast transformation techniques and is not suitable for real-time processing. The techniques in the second category directly operate on the pixels. Contrast enhancement is one of the important image enhancement techniques in the spatial domain. Gray transformation is the simplest and most effective image enhancement method. Various authors have proposed various methods based on histogram equalization. Daeyeong, et al (2017) proposed an adaptive contrast enhancement algorithm considering both preservations of the shape of a one-dimensional (1-D) histogram and statistical information on the gray-level differences between neighboring pixels obtained by a 2-D histogram. Veluchamy, M., and Subramani, B. (2020) proposed an efficient method called fuzzy dissimilarity adaptive histogram equalization with gamma correction. Pal and King (1980) proposed a method of image enhancement by computer using the fuzzy set theoretic approach. They used Zadeh's intensification operator (an S-sharp function) in membership modification. Yang Ciyin, and Huang Lianqing (2002) proposed a kind of sine nonlinear grey level transformation. According to the characteristics of the infrared images, Gong et al., (2012) proposed an image enhancement method based on sine grayscale transformation (an S-sharp function). Jose-Luis Lisani

(2020) proposed the technique based on a logarithmic mapping function. Zhang and Feng (2020) proposed an image enhancement algorithm based on a quadratic function (an S-sharp function) for gray value stretching.

This paper proposes an image enhancement method based on an S-sharp function of grayscale transformation and neighborhood information. The image enhancement method consists of 3 steps: establish function, add image threshold into function, and modify the result using pixel neighborhood information. This method achieves a good performance in the experiment.

METHODOLOGY

2.1 An improved sine grayscale transformation

Gong et al. (2012) proposed an improved sine grayscale transformation. The transformation function is written as follows:

$$f(x_{i,j}) = \begin{cases} (x_{i,j} - a)[\sin(\frac{x_{i,j} - a}{q - a})]^{k_{i,j}} + a, & a \le x_{i,j} \le q \\ (x_{i,j} - b)[\sin(\frac{x_{i,j} - q}{b - q})]^{k_{i,j}} + b, & q < x_{i,j} \le b \end{cases} \quad \textbf{(1)}$$

In formula (1), a is the minimum of pixels gray, b is the maximum of pixels gray, q is image threshold, $k_{i,j} = \alpha \times \frac{|x_{i,j} - \overline{x_{i,j}}|}{\overline{x_{i,j}}}$, a is a constant, $\overline{x_{i,j}}$ is the average grayscale of pixels in window W_t, $\overline{x_{i,j}} = \frac{1}{m}\sum_{i,j \in W_t} x_{i,j}$, m is the size of window W_t.

2.2 Gray transformation function based on the quadratic function

Zhang and Feng (2020) proposed an image enhancement algorithm based on a quadratic function for gray value stretching in which the gray value of images is self-adjusted with two quadratic functions. The function defined as follows:

$$f(x_{i,j}) = \begin{cases} a, & x_{i,j} = a \\ \frac{(x_{i,j} - a)^2}{q - a} + a, & a \le x_{i,j} \le q \\ -\frac{(x_{i,j} - b)^2}{b - q} + b, & q < x_{i,j} \le b \\ b, & x_{i,j} = b \end{cases} \quad \textbf{(2)}$$

In formula (2), a is the minimum of pixels gray, b is the maximum of pixels gray, q is image threshold.

2.3 Neighborhood standard deviation

Image $I=\{x_{i,j}\mid i=1,2,3,\cdots,m,\ j=1,2,3,\cdots,n\}$, where $x_{i,j}$ is the grayscale of the pixel in row i and column j of the image. Now, $\sigma=\mathrm{SD}(a,b,c,d)$ denotes the standard deviation of a,b,c,d. σ_{ij} is the neighborhood standard deviation of the pixel inrow i and column j. According to the location of each pixel in the image (edge and non-edge), the σ_{ij} is calculated as follows:

$$\sigma_{ij}=SD\begin{pmatrix} x_{i-1,j-1} & x_{i-1,j} & x_{i-1,j+1} \\ x_{i,j-1} & x_{i,j} & x_{i,j+1} \\ x_{i+1,j-1} & x_{i+1,j} & x_{i+1,j+1} \end{pmatrix}, \quad \begin{matrix} 2<i<m-1 \\ 2<j<n-1 \end{matrix},$$

$$\sigma_{i1}=SD\begin{pmatrix} x_{i-1,1} & x_{i-1,2} \\ x_{i,1} & x_{i,2} \\ x_{i+1,1} & x_{i+1,2} \end{pmatrix}, \quad 1<i<m, \qquad \sigma_{1j}=SD\begin{pmatrix} x_{1,j-1} & x_{1,j} & x_{1,j+1} \\ x_{2,j-1} & x_{2,j} & x_{2,j+1} \end{pmatrix}, \quad 1<j<n,$$

$$\sigma_{in}=SD\begin{pmatrix} x_{i-1,n-1} & x_{i-1,n} \\ x_{i,n-1} & x_{i,n} \\ x_{i+1,n-1} & x_{i+1,n} \end{pmatrix}, \qquad \sigma_{mj}=SD\begin{pmatrix} x_{m-1,j-1} & x_{m-1,j} & x_{m-1,j+1} \\ x_{m,j-1} & x_{m,j} & x_{m,j+1} \end{pmatrix},$$

$$\sigma_{11}=SD\begin{pmatrix} x_{1,1} & x_{1,2} \\ x_{2,1} & x_{2,2} \end{pmatrix}, \sigma_{1n}=SD\begin{pmatrix} x_{1,n-1} & x_{1,n} \\ x_{2,n-1} & x_{2,n} \end{pmatrix}, \sigma_{m1}=SD\begin{pmatrix} x_{m-1,1} & x_{m-1,2} \\ x_{m,1} & x_{m,2} \end{pmatrix}, \sigma_{mn}=SD\begin{pmatrix} x_{m-1,n-1} & x_{m-1,n} \\ x_{m,n-1} & x_{m,n} \end{pmatrix}$$

2.4 Define a S∗-sharp function

According to the image characteristics of sine function, the S∗-sharp function is established by magnifying and translating the sine function $f(x)=\sin(x), x\in[-\pi/2,\pi/2]$. The S∗-sharp function as follow:

$$f(x_{i,j})=255\times\frac{1}{2}\times[\sin(\frac{x_{i,j}}{255}\times\pi-\frac{\pi}{2})+1] \qquad (3)$$

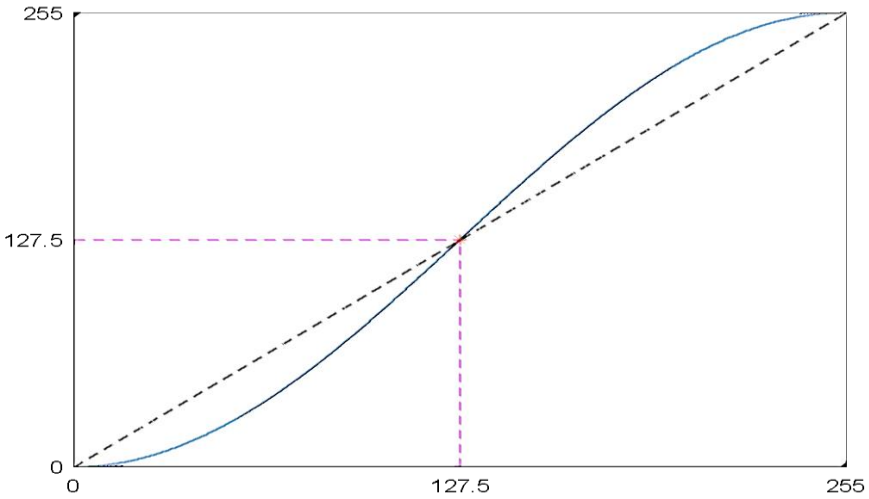

Figure 1. S∗-sharp function

2.5 Add image threshold into the S∗-sharp function(S-sharp function)

The S-sharp function in formula (3) has an inflection point at (127.5,127.5). In Fig. 1, the S-sharp function makes the grayscale smaller when they are less than 127.5, and makes the grayscale bigger when they are more than 127.5. To use the inflection point of formula (3) more flexibly, now the inflection point is corresponding to the image threshold (T). A variant of formula (3) is carried as follow:

$$f(x_{i,j})=\begin{cases} T\times[\sin(\frac{x_{i,j}}{T}\times\frac{\pi}{2}-\frac{\pi}{2})+1], & 0\le x_{i,j}\le T \\ (255-T)\times\sin(\frac{x_{i,j}-T}{255-T}\times\frac{\pi}{2})+T, & T<x_{i,j}\le 255 \end{cases} \quad (4)$$

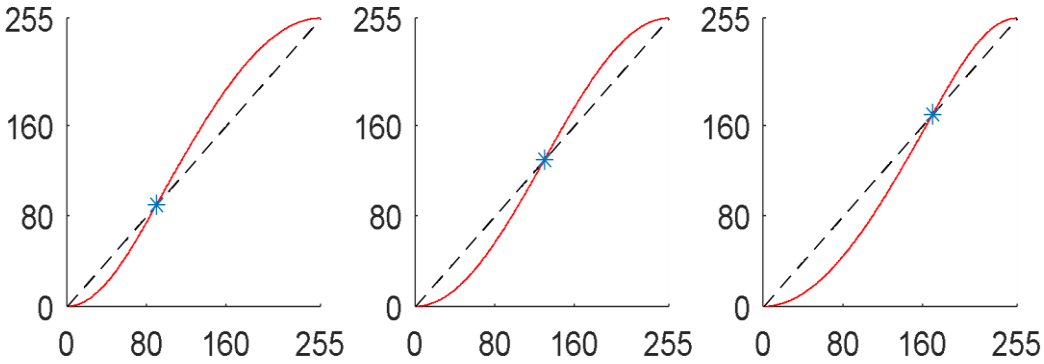

Figure 2. S-sharp function （T=90, 130, 170）

2.6 Modify the grayscale base on pixel neighborhood information

Using formula (4), the same grayscale in the input image corresponds to the same gray value in the output image. Now, for each pixel grayscale processed by formula (4), we modify the pixel grayscale base on its neighborhood information(σ_{ij}). In the input image, for the pixel $x_{i,j}$, the larger the value of σ_{ij} shows the pixel grayscales in pixel $x_{i,j}$'s neighborhood changing strongly.

This study proposes the image enhancement method (we note **NIEM**) consists of two steps. The two steps are as follows:

Step 1: Compute $f(x_{i,j})$ using formula (4);

Step 2: Modify the $f(x_{i,j})$. Move $f(x_{i,j})$ vertically towards $y=x$, so that the distance from $y=x$ is b times as much as the original ($0\le b\le 1$), and get $y_{i,j}$. Where parameter b and σ_{ij} are negatively correlated.

In experiments, parameter b is computed by a function with σ_{ij}. Fig.3 shows that the change of grayscale (0 ~ 255) at different parameter b.

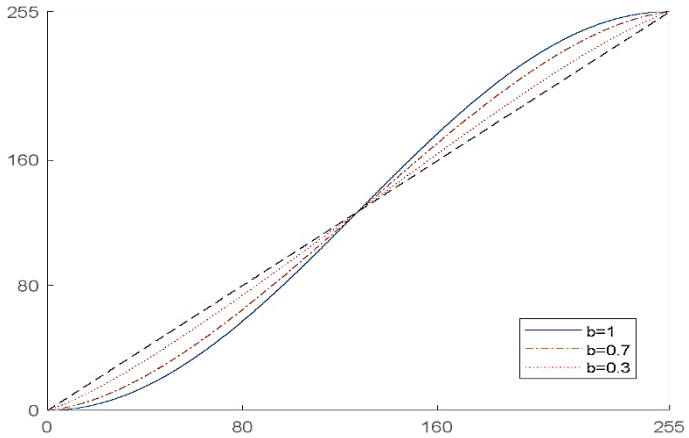

Figure 3. An example of S-sharp function modified by b = 0.3,

EXPERIMENTAL RESULTS AND DISCUSSION

This study uses Mean Squared Error (MSE), Peak Signal-Noise Ratio (PSNR), and Structural Similarity Index Measure (SSIM) to evaluate the image enhancement effect. The smaller MSE or the higher PSNR (SSIM) indicates a better enhancement effect (Thung and Raveendran, 2009).

$$MSE = \frac{1}{M \times N} \sum_{i=1}^{M} \sum_{j=1}^{N} (x_{i,j} - y_{i,j})^2 \quad (5)$$

$$PSNR = 10 \times \log_{10} \frac{(2^n - 1)^2}{MSE} dB \quad (6)$$

$$SSIM(x, y) = \frac{(2\mu_x\mu_y + c_1)(2\sigma_{xy} + c_2)}{(\mu_x^2 + \mu_y^2 + c_1)(\sigma_x^2 + \sigma_y^2 + c_2)} \quad (7)$$

In formula (6), n = 8 (the test image is an 8bits image). In formula (7), μ_x is the mean of x, μ_y is the mean of y, σ_x^2 is the variance of x, σ_y^2 is the variance of y, σ_{xy} is the covariance of x and y. c_1 and c_2 are constants (Wang et al., 2004; Wang and Simoncelli, 2011).

In this section, the test image(**Lena** and **Pout)** processed by enhancement methods including formula (1)(set α = 10), (2), (3), (4), and **NIEM**. In experiments, the threshold T is computed by the Otsu method (Otsu, 1979), then the parameter b value under the gray level of each pixel is calculated by formula (8).

$$b = b_{ij} = \begin{cases} \ln[e - \frac{\sigma_{ij} - \sigma_{\min}}{\sigma^* - \sigma_{\min}} \times (e - e^{\frac{1}{2}})], & \sigma_{ij} \le \sigma^* \\ \ln[e^{\frac{1}{2}} - \frac{\sigma_{ij} - \sigma_{\max}}{\sigma^* - \sigma_{\max}} \times (e^{\frac{1}{2}} - e^{\frac{1}{3}})], & \sigma_{ij} > \sigma^* \end{cases} \quad (8)$$

Where $\sigma^* = SD$ (all pixels in image), $\sigma_{\min} = \min\{\sigma_{ij} \mid i = 1,2,3,\cdots,m,\ j = 1,2,3,\cdots,n\}$, $\sigma_{\max} = \max\{\sigma_{ij} \mid i = 1,2,3,\cdots,m,\ j = 1,2,3,\cdots,n\}$.

Table 1. PSNR, MSE, and SSIM values

	Image Lena				
	(a,b)	(a,c)	(a,d)	(a,e)	(a,f)
PSNR	20.5951	21.6286	22.6591	22.5440	**22.9350**
MSE	566.9886	446.9082	352.5062	361.9781	**330.8151**
SSIM	0.7965	0.9341	0.9301	0.9365	**0.9451**
	Image Pout				
	(a,b)	(a,c)	(a,d)	(a,e)	(a,f)
PSNR	24.4769	26.2251	24.3008	26.1890	**26.9218**
MSE	231.9457	155.0835	241.5456	156.3794	**132.0988**
SSIM	0.7339	0.9521	0.9483	0.9551	**0.9604**
Note: a is original image, b is processed by formula (1), c is processed by formula (2), d is processed by formula (3), e is processed by formula (4), f is processed by **NIEM**.					

Table 1 shows that compared with other algorithms, **NIEM** gets the smallest MSE and the highest PSNR, SSIM. In image Lena test, MSE value:330.8151, PSNR value:22.9350, and SSIM value: 0.9451. In image Pout test, MSE value:132.0988, PSNR value:26.9218, and SSIM value: 0.9604. This means that NIEM gets better performance than the other four methods. The SSIM value processed by formula (3), (4), and NIEM is gradually rising, so that it is necessary and effective to add threshold and image neighborhood information. In Fig.4, Fig.4(b) and Fig.4(c) are over-enhanced and Fig.4(f) and the original image are visually more similar. In conclusion, NIEM image enhancement method, which not only can use S-sharp functions for grayscale transformation but also consider the neighborhood information (standard deviation: σ_{ij}) of each pixel, is a more flexible and efficient algorithm. In the future study, image histogram will be used as image information in the image enhancement method.

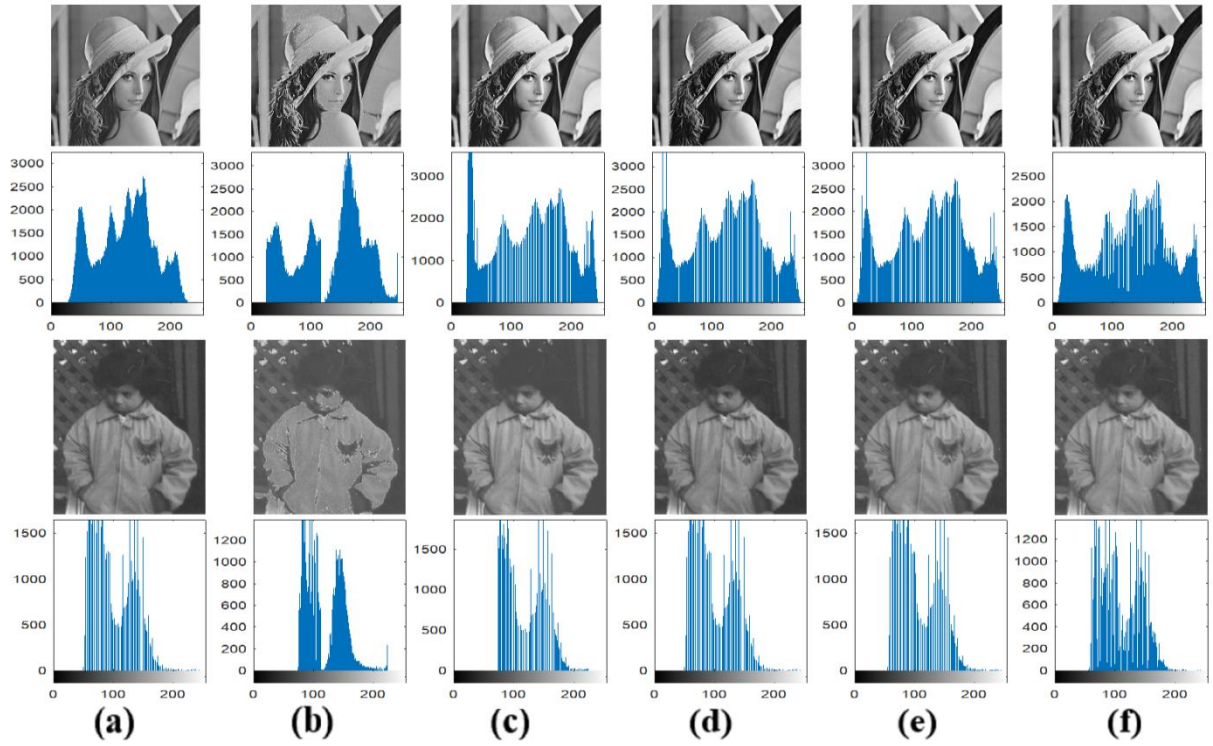

Figure. 4. (a) is the original image Pout, (b) is processed by formula (1), (c) is processed by formula (2), (d) is processed by formula (3), (e) is processed by formula (4), (f) is processed by **NIEM.**

REFERENCES

Daeyeong, Kim, Changick, and Kim. (2017) Contrast enhancement using combined 1-d and 2-d histogram-based techniques. IEEE Signal Processing Letters, 24(6), 804-808.

Magudeeswaran Veluchamy, Bharath Subramani. (2020) Fuzzy dissimilarity color histogram equalization for contrast enhancement and color correction. Applied Soft Computing, 89(1):106077.

Pal, S. K. and King, R. A. (1980) Image enhancement using fuzzy set, Electronics letters 16(10), 376-378.

Yang Ciyin, Huang Lianqing. (2002) X-ray image enhancement based on sinusoidal grayscale transformation. Optical Technology, 05,407-408.

Gong, C., Luo, C. and Yang, D. (2012) Improved image enhancement algorithm based on sine gray level transformation. Video Engineering 13, 60–63.

Lisani, J. L. . (2020) Local contrast enhancement based on adaptive logarithmic mappings. Image Processing On Line, 10, 43-61.

Zhang, Y. R. K. Y. and Feng, C. (2020). Image enhancement algorithm based on quadratic function and its implementation with fpga. Modern Electronics Technique 43(8), 72-76,81.

Thung, K.-H. and Raveendran, P. (2009) A survey of image quality measures. 2009 international conference for technical postgraduates (TECHPOS), IEEE, pp. 1-4.

Wang, Z., Bovik, A. C., Sheikh, H. R. and Simoncelli, E. P. (2004) Image quality assessment: from error visibility to structural similarity. IEEE transactions on image processing 13(4), 600-612.

Wang, Z., Bovik, A. C., Sheikh, H. R. and Simoncelli, E. P. (2011) The ssim index for image quality assessment, http://www.cns.nyu.edu/ lcv/ssim/ (https://ece.uwaterloo.ca/~z70wang/research/ssim/).

Otsu, N..(1979) A threshold selection method from gray-level histograms. IEEE Transactions on Systems, Man, and Cybernetics, 9(1), 62-66.

BorneoScience
The Journal of Science & Technology
Volume 42 Issue 1 : March 2021
Online ISSN : 2231-9085 | ISSN : 1394-4339

ASCORBIC ACID DETERMINATION IN FRESH AND COMMERCIAL FRUIT JUICES BY DIFFERENTIAL STRIPPING VOLTAMMETRIC TECHNIQUE AT A GLASSY CARBON ELECTRODE

Nur Syamimi Zainudin* and Zaihasra Azis

[1]Faculty of Applied Sciences, Universiti Teknologi MARA Pahang, Jengka Campus, 26400 Bandar Tun Abdul Razak Jengka, Pahang, Malaysia

** Corresponding author. Email: nursyamimizainudin@uitm.edu.my*

Received 1st April 2021; accepted 8th July 2021.
Available online 12 August 2021
DOI: https://doi.org/10.51200/bsj.v42i1.4458

ABSTRACT. *Ascorbic acid, also known as Vitamin C cannot be synthesized by humans. Ascorbic acid is commonly found in a variety of vegetables and fruits such as mangoes, oranges, broccolis and lettuce. Hence, vegetables and fruits become the main sources of ascorbic acid to meet dietary intake. The differential pulse anodic stripping voltammetry (DPASV) technique using glassy carbon electrode (GCE) as a working electrode and phosphate buffer at pH 4.2 as a supporting electrolyte has been proposed for ascorbic acid determination in natural and commercial fruit juices. The optimum instrumental conditions for electroanalytical determination of ascorbic acid by the proposed DPASV technique were initial potential (E_i) = 0 V, end potential (E_f) = 0.8 V, accumulation time (t_{acc}) = 60 s, scan rate (v) = 0.125 V/s and pulse amplitude = 0.150 V. The anodic peak appeared at 0.3598 V. The curve was linear from 0.028 to 1.703 mM (R^2=0.9999) with a detection limit of 0.0114 mM. The precisions in terms of relative standard deviation (RSD) were 1.30%, 0.50% and 0.06%, respectively. The ruggedness of the proposed DPASV technique was tested with statistical F-test. Satisfactory recoveries ranging from 73.65±1.70% to 101.93±1.65% were obtained for three different known concentrations of AA in the fruit juice samples. It can be concluded that the proposed technique is precise, accurate, rugged, low cost, fast and has the potential to be an alternative method for routine analysis of ascorbic acid in natural and commercial fruit juices*.

KEYWORDS*:* Ascorbic Acid, Commercial Fruit Juice, Glassy Carbon Electrode, Voltammetry

INTRODUCTION

Ascorbic acid (AA) was discovered in the twentieth century in 1907 by Holst and Frolich, as a solution for scurvy disease. During that year, the disease had been reported to be 'ship beriberi'. An experiment was carried out on guinea pigs by feeding them with fresh apples, fresh potatoes, fresh cabbage and fresh lemon juices which are high in the AA. The guinea pigs were also fed with a simple diet like oat, barley and wheat. The results indicated that deficiency of AA caused scurvy (Packer & Fuchs, 1997). The AA is important for collagen production, a protein which gives structure to bones, cartilages, muscles and blood vessels as well as an antioxidant and free radical scavenger (Sona *et al*., 2015; Yilmaz *et al*., 2008). The AA also helps in iron absorption and maintains capillaries, bones and teeth (Pisoschi *et al*., 2011). The main natural sources of AA are various fruits and vegetables

especially kiwi, mangoes, papayas, lettuce, tomatoes, peppers, strawberries, cantaloupe and broccolis (Sadia *et al*., 2014). The AA is also known as vitamin C, L-ascorbic and 2,3-didehydro-L-threohexono-1,4-lactone as well as 3-keto-L-gulofuranolactone. It has a chemical formula of $C_6H_8O_6$ and a molecular weight of 176 $gmol^{-1}$ while its chemical structure is shown in Figure 1.

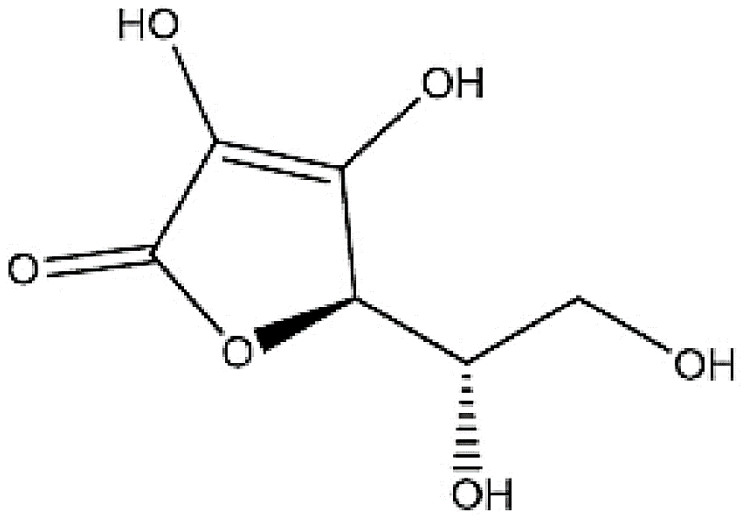

Figure 1: Chemical structure of ascorbic acid

The AA content tends to be lost during processing, storing and packaging since it is highly sensitive to light, heat, temperature and oxygen (Gazdik *et al*., 2008). Storage of commercial fruit juices in closed containers at ambient temperature for four months showed that the AA loss ranged from 29% to 41% (Morris *et al*., 2011). Meanwhile, in open containers and in the refrigerator for 31 days, the loss of AA was about 60% to 67%. About 12.5% of AA content has been lost for the commercial fruit juice in open containers which was stored outside the refrigerator for 10 days (Morris *et al*., 2011). For the same period, about 9% of the AA content has been lost for refrigerated commercial fruit juices (Morris *et al*., 2011). Hence, it is very important to have a simple, very sensitive, precise, accurate, rugged, low cost and fast method for determining the exact content of AA in the natural and commercial fruit juice in the markets.

Various analytical techniques have been applied for AA determination such as chromatographic method, particularly high-performance liquid chromatography (HPLC) (Klimczak *et al*., 2015; Tyagi *et al*., 2014; Valente *et al*., 2011), titrimetric method (Tareen *et al*., 2015; Nweze *et al*., 2015; Dioha *et al*., 2011)**,** spectrometric method (Liamas *et al*., 2011). However, HPLC method uses expensive equipment, requires a tedious sample pre-treatment, uses of toxic organic solvent as mobile phase and various harmful reagents (Zhang *et al*., 2018). In the titrimetric method, difficulties are encountered with titrants and interferences often occur with coloured samples which lead to lack of specificity (Sona *et al*., 2015). Meanwhile, in direct spectrophotometry, there is a matrix effect in the ultraviolet (UV) region since many organic compounds in samples may also exhibit UV absorbance during measurement (Ogunlesi *et al*., 2010). In addition, the spectrophotometry is beyond the specific limit and the intensity of absorption is not directly proportional to the concentration (Raghu *et al*., 2007).

Differential pulse voltammetric (DPV) technique has been used to determine AA in fruit juices and wine based on its oxidation at carbon paste electrodes (Pisoschi *et al*., 2011). Cyclic and square wave voltammetric techniques were also used for electrochemical behaviour investigation and determination of AA at a glassy carbon electrode in which the methods were tested in some beverages and fresh edible vegetables (Aabraha & Sargawie, 2014). Determination of AA in real samples of tropical fruits was carried out by cyclic voltammetric technique using glassy carbon electrode in phosphate buffer at pH 2 (Okiei *et al*., 2009).

Differential pulse stripping voltammetric (DPSV) technique has good discrimination against capacitive current which resulting in improved resolution, higher sensitivity, low detection limit and effectiveness to be applied in the analysis of various electrochemically active compounds at their trace amounts at a reasonable cost and through a simple and fast analysis (Skrovanko *et al*., 2015). The purpose of this study is to optimize and validate a proposed differential pulse anodic stripping voltammetric (DPASV) technique using bare glassy carbon electrode as a working electrode and phosphate buffer solution (pH 4.2) as a supporting electrolyte for quantitative analysis of AA in the several commercial and fresh fruit juices.

METHODOLOGY

Materials

All chemicals used were analytical grade reagents. The AA standard (MW = 176 g mol^{-1}) with 99% purity was obtained from Sigma Aldrich, UK. All solutions were prepared in deionized water. For the preparation of 2.84 mM AA stock solution, the AA powder was dissolved in a 100 mL volumetric flask. The standard working solution series were prepared by carrying out dilution of the 2.84 mM stock solution. All prepared stock and standard working solutions were protected from light and used within 24 hours to avoid decomposition. Phosphate buffer solution (PBS) was prepared by adding and dissolving 2.70 mL of ortho phosphoric acid, 27.218 g of potassium dihydrogen phosphate, 71.630 g disodium hydrogen phosphate in the 1000 mL of volumetric flask. Sodium hydroxide with a concentration of 0.1 M was used to adjust the pH of the PBS solution to the 4.2 (Pisoschi *et al*., 2011).

Instrumentation

The voltammetric determination was carried out using Autolab Potentiostat (Metrohm, Switzerland) that consisted of a three-electrodes system. A glassy carbon electrode (GCE) as the working electrode (WE), a platinum wire as the counter electrode (CE) and an Ag/AgCl (3M KCl) as the reference electrode (RE). The GCE was polished with alumina on an alumina pad and then rinsed with deionized water before being used for measurements. The Autolab Potentiostat was connected to a computer, installed with NOVA 1.1 software for information processing. The pH meter (Hanna Instruments, UK) was employed for all pH measurements.

Voltammetric measurement

Validation of proposed DPASV technique

The validation of the proposed DPASV technique was carried out by applying optimum operational instrumental parameters applied were initial potential (E_i) = 0 V, final potential (E_f) = 0.8 V,

accumulation time (t_{acc}) = 60 s, scan rate (v) = 125 mV/s, accumulation potential (E_{acc}) = 0 mV and pulse amplitude = 150 mV, as previously studied by Nur Syamimi *et al*, (2020).

An appropriate linearity range with acceptable correlation coefficient (R^2), limit of detection (LOD), limit of quantification (LOQ), precision, accuracy, ruggedness and recovery of spiked AA standard into the commercial and fresh fruit juices were analyzed in order to verify the suitability of the proposed DPASV technique for AA determination as proposed by Miranda *et al,* (2012). The linearity was investigated in the range of 0.028 to 1.703 mM AA standard solution in the electrochemical vessel. The LOD was estimated by additional lower concentration of the AA standard solution until obtaining a response that was significantly different from the response of PBS solution at pH 4.2. The LOQ was calculated by the equations; LOD = 3 SD/m and the value of the LOQ was 3.333 times the value of the obtained LOD.

Three different concentrations (0.028, 0.284 and 0.852 mM) of AA standard solution were applied for intra-day and inter-day precision with three replicate measurements (n=3). The precision of the proposed DPASV technique was determined in terms of the relative standard deviation (RSD). The accuracy of the proposed DPASV technique was examined by spiking the three known volumes of AA standard solution which gave a final concentration of 0.028, 0.284 and 0.852 mM in the electrochemical vessel. The actual concentrations of AA standard solution found in the electrochemical cell by the proposed DPASV technique were calculated using the regression equation achieved in linearity range study. The ruggedness of the proposed DPASV technique was investigated with three replicate (n=3) measurements using the same instrument (Metrohm, Autolab Potentiostat) which operated by two different analysts under the same optimum parameters. Statistical *F*-test was carried out for the ruggedness.

Collection and preservation of fruit juices

Blackcurrant, orange, mango, lychee and guava commercial fruit juices were bought at the nearest mart in Jengka, Pahang. All these commercial fruit juices were centrifuged before being analyzed by the proposed DPASV technique (Pisoschi *et al*., 2011). Meanwhile, an average-sized pineapple and orange, also bought in Jengka, Pahang was peeled and pressed. The obtained pineapple and orange juice were then being centrifuged and analyzed within one hour after the sample preparation in order to avoid degradation of AA which could contribute to inaccurate voltammetric measurements.

Recovery studies of spiked AA standard in fruit juices

The recovery of AA standard solution in the fruit juices (by pressing) and commercial fruit juices was determined by spiking 1.0 mL of the juices into the measuring cell containing PBS solution at pH 4.2. This study was carried out with three replicates (n=3). Recovered concentrations of the spiked AA standard solution in the samples were calculated using the regression equation from a calibration curve and from the following formula;

$$\text{Recovery (\%)} = (Q_{DET} - Q_P) / Q_{ADD} \times 100$$

Where, Q_{DET} represents concentration of AA determined in the juices, Q_P represents concentration of AA previously present in the juices and Q_{ADD} represents the concentration of AA added in the juices.

RESULTS AND DISCUSSION

Validation of the proposed DPASV technique

Linearity, limit of detection (LOD) and limit of quantification (LOQ)

The constructed calibration curve was linear from 0.028 mM to 1.703 mM with equation of I_p (nA) = 19337x – 219.4 at 14 different concentrations of the AA, as represented in Figure 5. The acceptable correlation coefficient (R^2) had been achieved, which was 0.9999. The LOD was 0.0114 mM and the LOQ was 0.0379 mM.

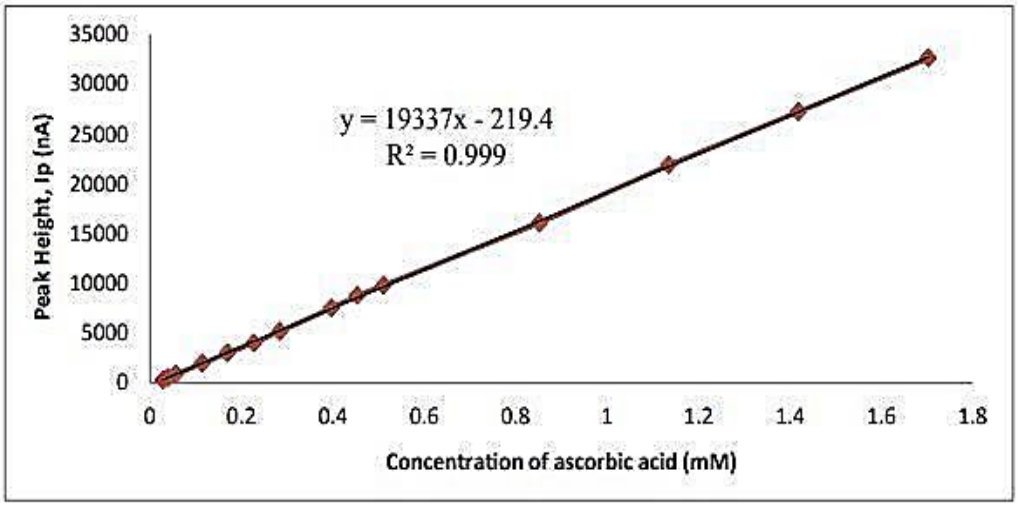

Figure 5: Linear curve of I_p against concentrations of AA in phosphate buffer solution pH 4.2

Precision

The precision of the proposed DPASV technique for AA analysis in terms of RSD was determined using 0.028 mM, 0.284 mM and 0.852 mM AA standard solution in three replicates (n=3) measurements. The RSD values obtained were 1.30%, 0.50% and 0.06% for respective concentrations. The proposed DPASV technique was considered precise as the obtained RSD values were less than 2% (Ngai *et al*., 2013).

Accuracy

The recoveries of 93.58%, 98.54% and 98.78% were respectively achieved for the spiked concentrations of 0.028 mM, 0.284 mM and 0.852 mM AA standard solution, as shown in Figure 6. These results indicate that the proposed DPASV technique was considered accurate since satisfactory recoveries were successfully achieved (Radi *et al*., 2011).

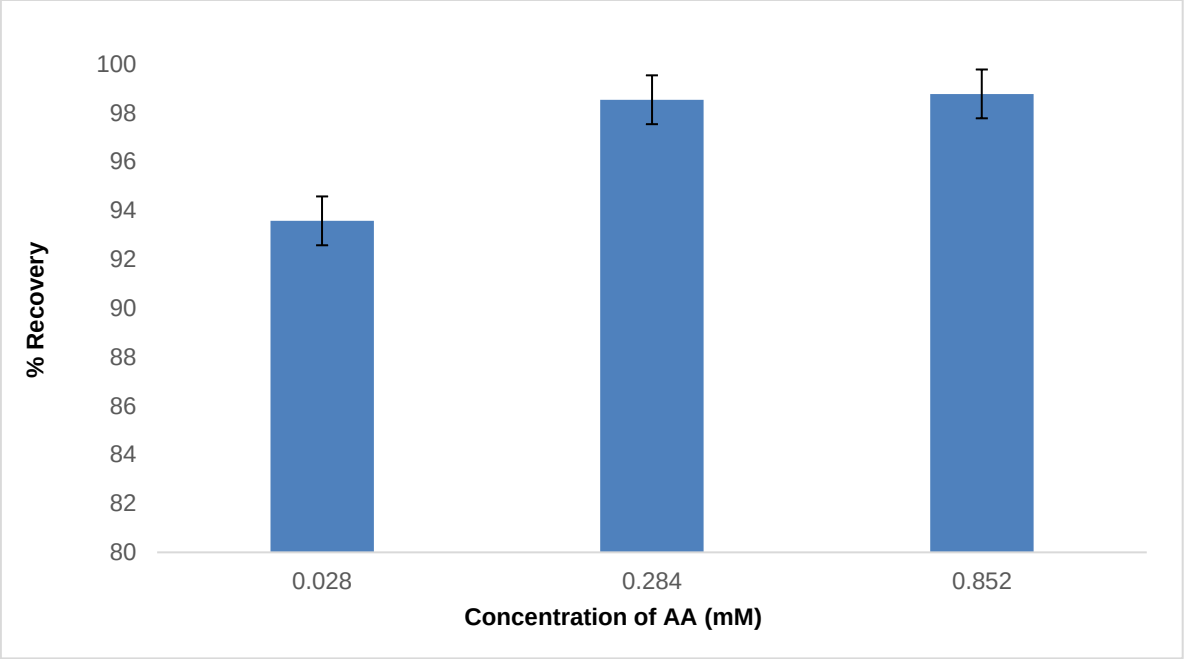

Figure 6: Recoveries (%) for three different known concentrations of AA standard solution

Ruggedness

The RSD values of 1.27%, 2.93% and 0.50%, respectively for 0.028 mM, 0.284 mM and 0.852 mM AA standard solution were achieved for the measurements by the first analyst. Otherwise, 0.91%, 0.07% and 0.07% of RSD achieved for measurements conducted by the second analyst, also for respective AA concentrations (Jain & Rather, 2011). There were no significant differences between the obtained variances for AA when the measurements were conducted by two different analysts with the same instrument (Metrohm, Autolab Potentiostat) at the 5% significance level, as proved by two-tailed *F*-test. The proposed DPASV technique was considered to be rugged.

Recovery and determination of AA in fruit juices

The recoveries achieved for AA content in blackcurrant, orange and mango commercial fruit juices were 80.00±6.25%, 73.65±1.70% and 97.48±16.90%. Meanwhile, the recovery of 101.93±1.65% was obtained for fresh pineapple juices, as shown in Table 1. According to *t*-test, there were no significant differences between recovery and spiked value at the 95% confidence level since all the calculated *t* values are lower than the theoretical *t* value, which was 4.303 (Bergamini *et al*., 2010). These satisfactory recoveries also indicated that the matrix did not affect the measurement of the AA in the fruit juices by the proposed DPASV technique.No AA was detected in both lychee and guava commercial fruit juices. Tables 2 and 3 show the content of AA in the blackcurrant, orange and mango commercial fruit juices were 2.0213 mM, 1.8286 mM and 2.9798 mM, respectively. On the other hand, the content of AA in the fresh orange and pineapple juices were 0.8000 mM and 0.698 mM. The AA content in the commercial fruit juices much higher compared to the fresh fruit juices might be due to the AA enrichment during the commercial fruit juices processing.

Table 1: Recovery for spiked AA standard solution in the fruit juices (n=3)

Samples	Spiked Concentration of AA Standard Solution (mM)	Found Concentration of AA Standard Solution (mM)	Recovery (%)	Average Recovery ± SD (RSD)
Blackcurrant (Commercial Fruit Juice)	0.0852	0.0760 0.0653 0.0709	89.19 76.69 83.24	80.00±6.25 (7.8 %)
Orange (Commercial Fruit Juice)	0.0852	0.0611 0.0638 0.0634	71.71 74.86 74.38	73.65±1.70 (2.31 %)
Mango (Commercial Fruit Juice)	0.0852	0.0799 0.0987 0.0705	93.86 115.90 82.69	97.48±16.90 (17.34 %)
Pineapple (Fresh Fruit Juice)	0.0390	0.0402 0.0400 0.0390	102.95 102.85 100.03	101.93±1.65 (1.62 %)

Table 2: AA content in the commercial and fresh fruit juices

Samples	AA Content (mM)	AA Content (mg/100 cm^3)
Blackcurrant (Commercial Fruit Juice)	2.0213	35.59
Orange (Commercial Fruit Juice)	1.8286	32.24
Mango (Commercial Fruit Juice)	2.9798	52.52
Lychee (Commercial Fruit Juice)	Not detected	Not detected
Guava (Commercial Fruit Juice)	Not detected	Not detected
Orange (Fresh Fruit Juice)	0.800	14.10
Pineapple (Fresh Fruit Juice)	0.698	12.30

CONCLUSION

The proposed DPASV technique had been successfully applied to determine the AA in fruit juices. The present method had an advantage that a very simple sample pre-treatment was required. It was also found to be practically rapid, convenient, sensitive, accurate, precise, rugged and inexpensive. Therefore, it could be an excellent alternative method for the routine determination of AA in fruit juices in future.

ACKNOWLEDGEMENTS

We would like to thank the Faculty of Applied Sciences, UiTM Cawangan Pahang for providing the laboratory facilities and necessary support.

REFERENCES

Aabraha, T. & Sargawie, A. (2014). Assessment of some selected Beverages and Fresh Edible Vegetables as Nutritional Source of Vitamin C (Ascorbic Acid) by Cyclic and Square Wave Voltammetry. *International Journal of Science and Engineering Investigation 26*(3): 39-49.

Bergamini, M.F., Santos, D.P. & Zanoni, M.V.B. (2010). Determination of Major and Minor Elements in through ICP-AES. *Environmental Engineering and Management Journal 7*(6): 805-808.

De Lima, F., Gozzi, F., Fiorucci, A.R., Cardoso, C.A.L., Arruda, G.J. & Ferreira, V.S. (2011). Determination of linuron in water and vegetable samples using stripping voltammetry with carbon paste electrode. *Talanta 83*:1763-1768.

Dioha, I.J., Olugbemi, O., Onuegbu, T. & Shahru, Z. (2011). Determination of some tropical fruits by iodometric titration. *International Journal of Biological and Chemical Sciences 5*(5): 2180-2184.

Farahi, A., Lahrich, S., Achak, M., El Gaini, L., Bakasse, M. & El Mhammedi, M. A. (2014). Parameters affecting the determination of paraquat at silver rotating electrodes using differential pulse voltammetry. *Analytical Chemistry Research 1*: 16-21.

Gazdik, Z., Zitka, O., Petrlova, J., Adam, V., Zehnalek, J., Horna, A., Reznicek, V., Beklova, M. & Kizek, R. (2008). Determination of Vitamin C (Ascorbic Acid) Using High Performance Liquid Chromatography Coupled with Electrochemical Detection. *Sensors 8*: 7097–7112.

Geremedhin, W., Amare, M. & Admassie, S. (2013). Electrochemically pretreated glassy carbon electrode for electrochemical detection of fenitrothion in tap water and human urine. *Electrochimica Acta 87*: 749 – 755.

Jain, R. & Rather, J.A. (2011). Stripping voltammetry of tinidazole in solubilized system and biological fluids. *Colloids and Surfaces A: Physicochemical and Engineering Aspects 378*: 27-33.

Jain, R. & Sharma, S. (2012). Glassy carbon electrode modified with multi-walled carbon nanotubes sensor for the quantification of antihistamine drug pheniramine in solubilized systems. *Journal of Pharmaceutical Analysis 2*(1): 56-61.

Klimczak, I. & Gliszczy´nska-Swigło, A. (2015). Comparison of UPLC and HPLC methods for determination of vitamin C. *Food Chemistry 175*: 100–105.

Liamas, N.E., Nezio, M.S. & Band, B.S.F. (2011). Flow-injection spectrophotometric method with on-line photodegradation for determination of ascorbic acid and total sugars in fruit juices. *Journal of Food Composition and Analysis 24*: 127-130.

Okiei, W., Ogunlesi, M., Azeez, L., Obakachi, V., Osunsansi, M. & Nkenchar, G. (2009). The Voltametric and Titrimetric Determination of Ascorbic Acid Levels in Tropical Fruit Samples. *International Journal of Electrochemical Science 4*: 276-287.

Miranda, M. P., del Rio, R., del Valle, M. A., Faundez, M. & Armijo, F. (2012). Use of fluorine-doped tin oxide electrodes for lipoic acid determination in dietary supplements. *Journal of Electroanalytical Chemistry 668*: 1 – 6.

Morris, J.R., Bates, R.P. & Philip, G.G. (2001). Principles and Practices of small and medium scale fruit juice processing. United State.

Ngai, K.S, Tan, W.T, Zulkarnain, Z., Ruzniza, M.Z. & Mohammed, Z. (2013). Voltammetry Detection of Ascorbic Acid at Glassy Carbon Electrode Modified by Single-Walled Carbon Nanotube/Zinc Oxide. *International Journal of Electrochemical Science 8*: 10557-10567.

Nur Syamimi, Z., Norbaitina, S. & Megat, A.K.M.H. (2020). Validation and Determination of Ascorbic Acid in Multivitamin Tablets by Differential Pulse Anodic Stripping Voltammetric Technique at a Bare Glassy Carbon Electrode. *Malaysian Journal of Analytical Science 24* (6): 838-847.

Nur Syamimi, Z., Mohamad Hadzri, Y. & Noor Zuhartini, M.M. (2016). Voltammetric determination of Reactive Black 5 in waste water samples from the batik industry. *Malaysian Journal of Analytical Science 20*: 1254-1268.

Nweze, C.C., Abdulganitu, M.G & Erhabor, O.G. (2015). Comperative analysis of vitamin C in fresh fruit juices of Malusdomestica, Citrus Sinensi, AnanasComosus and CitrullusLanatus by Iodometric titration. *International Journal of Science 4*(1): 17-22.

Ogunlesi, M., Okiei, W., Azeez, L., Obakachi, V., Osunsanmi, M. & Nkenchar, G. (2010). Vitamin C Contents of Tropical Vegetables and Food Determined by Voltammetric and Titrimetric

Methods and Their Relevance to the Medical Uses of the Pants. *International Journal of Electrochemical Sciences 5*: 105-115.

Packer, L., and Fuchs, J. Vitamin C in health and disease. Marcel Dekker, Inc. New York, Basel, Hong Kong 1997.

Pisoschi, A.M., Pop, A., Negulescu, G.P. & Pisoschi, A. (2011). Determination of Ascorbic Acid Content of Some Fruit Juices and Wine by Voltammetry Performed at Pt and Carbon Paste Electrodes. *Molecules 16*: 1349-1365.

Radi A.E., Nassef, H.M. & El Basiony, A. (2011). Electrochemical behaviour and analytical determination of Reactive Red 231 on glassy carbon electrode. *Dyes and Pigments 99*: 924-929.

Raghu, V., Platel, K. & Srinivason, K. (2007). Comparison of Ascorbic Acid Content of Some Fruit Juices and Wine by Voltammetry Performed at Pt and Carbon Paste Electrodes. *Molecules 16*:1349-1365.

Sadia, G., Azizuddin., Rafi, A., Kousar, Y., Fareed, A. & Iftekhar, S. (2014). Determination of Ascorbic Acid Content of Some Capsicum Cultivars by Cyclic Voltammetry performed at GCE by External Standard Series Calibration Method. *International Journal of Electrochemical Science 9*: 5751-5762.

Sezgin, H., V., Dilgin, Y. & Gokcel, H., I. (2016). Adsorption and deposition-assisted anodic stripping voltammetry for determination of antimony (III) in presence of hematoxylin on glassy carbon electrode. *Talanta 164*: 677-683.

Sona, S., Jiri, M., Jiri, S., Mojmir, B., Jindrich, K. & Tunde, J. (2015). Determination of Ascorbic Acid by Electrochemical Techniques and other Methods. *International Journal of Electrochemical Science 10:* 2421-2431.

Skrovanko, S., Micek, J., Sochar, J., Baron, M, M Kynicky, J. & Jurikova, T. (2015). Determination of ascorbic acid by Electrochemical Technique and other methods. *International Journal of Electrochemical Sciences 10*: 2421-2431.

Tareen, H., Mengal, F., Masood, Z., Mengal, R., Ahmed, S., Bibi, S., Shoaib, S., Sami, U., Mandokhail, F., Riaz, M., Farhan, N & Nawaz, Z. (2015). Determination of vitamin c content in Citrus Fruits and in Non-Citrus Fruits by Titrimetric Method with Special Reference to their nutritional importance in human diet. *Biological Forum-An International Journal 7*(2): 367-369.

Tyagi, G., Jangir, D.K., Singh, R., Mehrotra, R., Ganaseran, R. & Gopal, E.S.R. (2014). Rapid determination of main constituents of packed juices by reverse phase-high performance liquid chromatography: an insight in to commercial fruit drinks. *Journal of Food Science and Technology 51*(3): 476–484.

Valente, A., Albuquerque, T.G., Ana, S.S. & Costa, H.S. (2011). Ascorbic acid content in exotic fruits. A contribution to produce quality data for food composition database. *Food Research International 44*: 2237-2242.

Yilmaz, S., Sadikoglu, M., Saglikoglu, G., Yagmur, S. & Askin, G. (2008). Determination of Ascorbic Acid in Tablet Dosage Forms and Some Fruit Juices by DPV. *International Journal of Electrochemical Science 3*: 1534-1542.

Zhang, Y., Zhou, W., Yan, J., Liu, M., Zhou, Y., Shen, X., Ma, Y., Feng, X., Yang, J. & Li, G. (2018). A review of the extraction and determination methods of thirteen essential vitamins to the human body: An update from 2010. *Molecules 23:* 1-25.

BorneoScience
The Journal of Science & Technology
Volume 42 Issue 1 : March 2021
Online ISSN : 2231-9085 | ISSN : 1394-4339

THE QUALITY ASSESSMENT OF HEAVY METALS IN MARINE SEDIMENTS FROM USUKAN COASTAL BEACH, KOTA BELUD, SABAH.

Ling Sin Yi[1], Junaidi Asis[1] & Baba Musta[1*]

[1]Geology Program, Faculty of Science and Natural Resources,
Universiti Malaysia Sabah, 88400 Kota Kinabalu, Sabah, Malaysia

** Corresponding author. Email: babamus@ums.edu.my*

Received 5th May 2021; accepted 24th July 2021.
Available online 12 August 2021
DOI: https://doi.org/10.51200/bsj.v42i1.4459

ABSTRACT. *A total of fifty-three (53) sediment samples were collected from Usukan coastal beach to study the potential of pollution due to heavy metals in the marine ecosystem. The sediment samples were collected along the coastal beach using a core sampler. The ICP-OES analysis was used to identify the concentration of heavy metals in the marine sediment samples. The results of pH analysis showed the increase of pH from 5.69 to 8.48 from inland into the sea. The lowest moisture content was 4.99%, whereas the highest was 48.75%. The organic matter ranges from 0.30 to 6.73%. The sediment texture varies from sandy, sandy loam, and sandy clay loam texture. The decreasing ranking order of heavy metals concentration is Fe (4476-29829 ppm) followed by Al (5803-8524 ppm) and Mn (103-504 ppm), which are still within the background values and standard limits. The assessment of Fe, Al and Mn contamination in sediment samples was performed by comparing with the allowable range of average background values and the standard limits from Sediment Quality Guideline (SQG) in marine sediment. In conclusion, the results of quality assessment using the geoaccumulation index (Igeo), contamination factor (CF), modified degree of contamination (mCd), and pollution load index (PLI) showed that the sediment from Usukan beach has a very low contamination level that causes only mild pollution.*

KEYWORDS. Geochemistry, Heavy Metal, Sediment Quality, Marine Environment

INTRODUCTION

The assessment of heavy metals quality in marine sediment is greatly affected by active chemical weathering or pedogenesis of the geological source rocks (Le'Pera *et al.*, 2001; Li *et al.*, 2019). Heavy metals found naturally in the Earth's crust and the rock-forming minerals are transported via rivers, surface run-offs, or any drainage system from the parent materials situated in areas with higher elevation and accumulate in the ocean basin. Besides topographical conditions, the tropical climate of the study area that experiences hot and wet seasons also lead to the transport and redistribution of heavy metals in marine sediments (Seaward and Richardson, 1989; Han *et al.*, 2001). When the heavy metal content exceeds the permissible level, the metals will increase the toxicity levels and contaminate the sediment (Zhang *et al.*, 2015; Jayamurali *et al.*, 2021). Heavy metals such as aluminium (Al), iron (Fe) and manganese (Mn) are released from lithogenic and anthropogenic sources that accumulate in the marine sediments, which also serve as a dynamic natural sink for the

pollutants (Chuan and Yunus, 2019). Thus, the coastal regions are selected to assess the sediment quality due to metal contamination.

Heavy metal pollution is a global concern as the contaminants are toxic and non-biodegradable, but instead accumulate in sediments which are then released into the seawater column and enter the food chains of marine organisms (Yang *et al.*, 2021; Xiang *et. al.*, 2021). The significant contribution of contaminants is from the terrestrial origin, such as natural processes and anthropogenic pollutant inputs via river discharge, land run-off, rapid industrialization, fishing or agricultural activities, and oil spills (Gopal *et al.*, 2017; Tchounwou *et al.*, 2012). All processes will lead to environmental or marine pollution and cause an imbalance in the global ecosystem. The concentrations of naturally occurring heavy metals vary according to the geological background (Vallius *et al.*, 2007; Wuana and Okeimen, 2011). Thus this has to be considered when assessing the degree of contamination in the study area. Therefore, Sediment Quality Guideline (SQG) is used as an appraisal to compare the concentrations of these elements to determine the quality and the eco-toxic level in marine sediments (Abolfazl and Ahmad, 2012; Birch, 2018). The profile and distribution of elements in sediments provide a record of depositional history, pollution origins, and the migration of the heavy metals to various parts of the marine sediments. The main objective of this research is to assess the distribution of selected heavy metal contamination in Usukan coastal beach by comparing with the permissible range of average background values and the standard limits established in the Sediment Quality Guideline (SQG).

DESCRIPTION OF STUDY AREA

The study area is located in Kota Belud, bounded by a latitude 6^0 17’ 40” N to 6^0 36’ 50” N and longitude 116^0 16’ 50” E to 116^0 33’ 0” E (Diagram 1). Kota Belud is formed from three major formations namely the Crocker Formation, which aged from Eocene to Early Miocene, Wariu Formation, which aged from Middle Miocene, and Quaternary Alluvium (Sanudin and Baba, 2007). The primary rock units underlying Kota Belud are interbedded sandstone and shale from Crocker Formation, and a mixture of fragmented rocks from different origins of Wariu Formation or melange. The Wariu Formation consists of argillite, breccia, metaclastics, micritic limestone, chert, spilite and ultramafic rocks from Wariu Formation (Collenette, 1958; Clement and Keij, 1958; Tongkul, 2006; Junaidi and Basir, 2012; Hall and Breitfeld, 2017). The Quaternary alluvium is originated from the weathered rocks from Crocker and Wariu Formation. The coral deposit aged from Pleistocene to Quaternary mainly occurred along the beach shoreline and nearby islands.

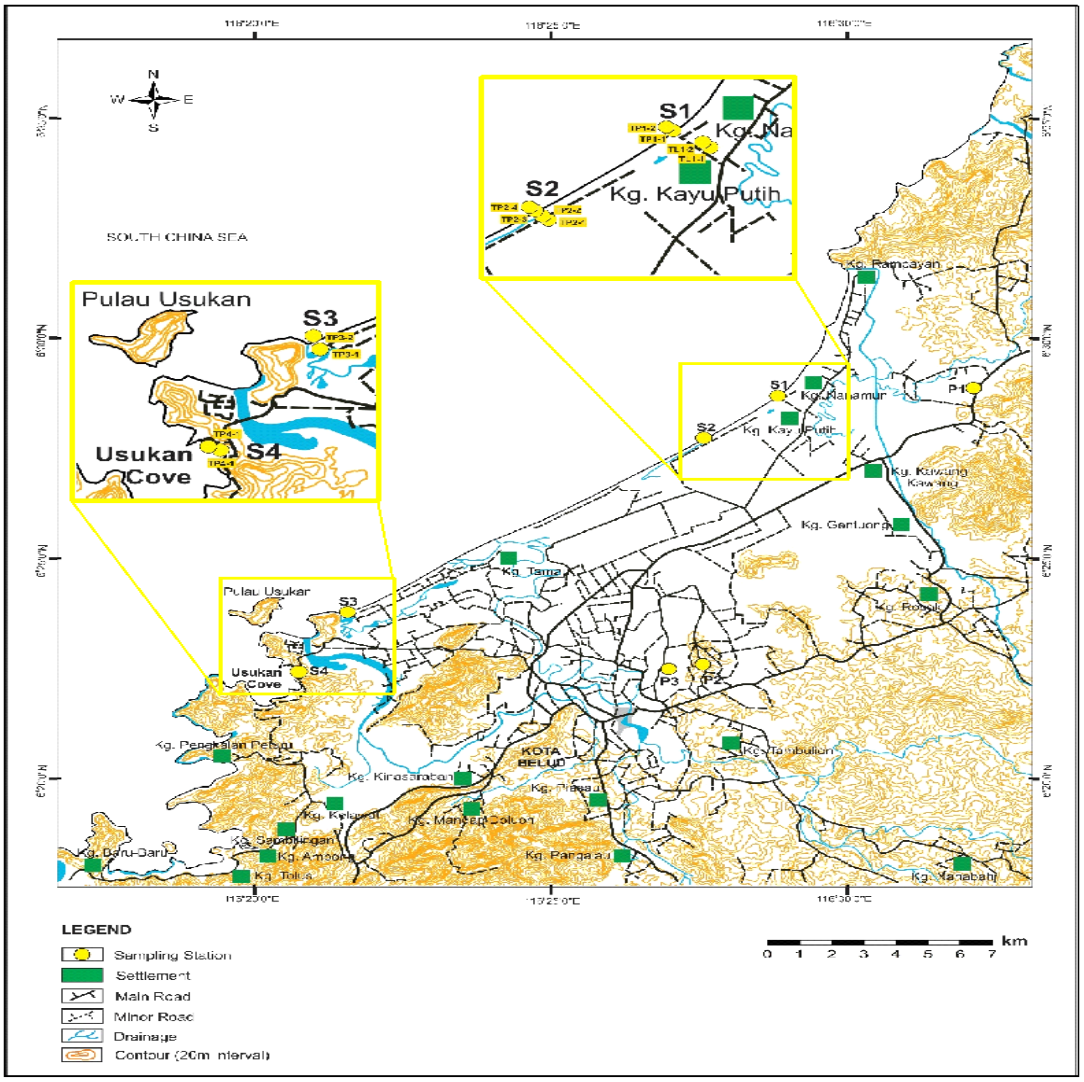

Diagram 1: Base map of the study area and sampling stations in Kota Belud, Sabah. (Source: Minerals and Geoscience Department of Malaysia, 2010)

MATERIALS AND METHODOLOGY

For this study, a total of fifty-three (53) sediment samples were collected from Usukan coastal beach. The sediments were collected as undisturbed samples in 100cm long PVC cores using the core sampler and were tightly closed with the PVC stopper. The sediments were then extruded from the PVC cores using the horizontal extrusion method before being segmented into every 10cm thick subsampling and kept in sealed ziplock bags for further laboratory analysis. The analyses conducted were pH, moisture content (MC), soil organic matter (SOM), and particle size distribution (PSD) to determine the physico-chemical characteristics of sediments based on the BSI technique (BSI, 1990). The pH analysis was conducted immediately once the samples were extruded. The samples for moisture content were dried at 105^0C for 8 hours using the conventional oven method, whereas the samples for SOM analysis were dried in the furnace overnight at 400^0C based on the dry combustion method. Air-dried samples were used for the particle size distribution (PSD) analysis using the dry sieving and pipette method. The heavy metal concentrations were determined using the aqua regia digestion method via Inductively Coupled Plasma-Optical Emission Spectrometry (ICP-OES) analysis using USEPA Method 6010D (Rev 4) (USEPA, 2014). The contamination levels of Al, Fe,

and Mn metals in the sediments were also evaluated using the Igeo, CF, mCd, and PLI statistical parameters to assess the sediment quality and were compared with the SQG and average background values (Turekian and Wedepohl, 1961).

RESULTS

Physico-Chemical Properties of Marine Sediments

Table 1 shows the pH value, moisture content, and organic matter in the sediment samples for every 10cm interval depth. The average pH readings for all sediments are within the range of 5.6-8.5. The average moisture content shows the lowest (4.9-5.8%) in the marine sediment profile (SP) as the samples are collected the furthest into land areas as compared to the core sediments (TP) (15.3-39.9%) and mud soil (TL) (35.4-48.8%) which are collected nearer to the sea. The SOM percentage shows the lowest range of 0.30-0.32% in SP, followed by 0.12-1.78% in TP and 4.66-6.73% in TL. The USDA textural classification shows SP and TP have sandy texture while TL has sandy loam and sandy clay loam texture, in which the grain size composition is shown in Diagram 2.

Table 1: Average values of pH, moisture content, and organic matter of sediments.

Samples	SP2	SP3	TP1-1	TP1-2	TP2-1	TP2-2	TP2-3	TP2-4	TP3-1	TP3-2	TP4-1	TP4-2	TL1-1	TL1-2
pH	5.7	6.5	7.1	7.9	7.3	7.8	7.9	7.5	7.3	7.7	8.4	8.5	6.1	6.4
MC %	5.0	5.8	25.0	25.8	24.0	23.8	15.3	25.3	26.2	39.9	25.9	27.9	35.4	48.8
OM %	0.3	0.3	0.3	0.3	0.2	0.2	0.2	0.1	0.3	0.8	1.6	1.8	4.7	6.7
Texture	Sandy	Sandy	Sandy	Sandy	Sandy	Sandy	Sandy	Sandy	Sandy	Sandy	Sandy	Sandy	Sandy loam	Sandy clay loam

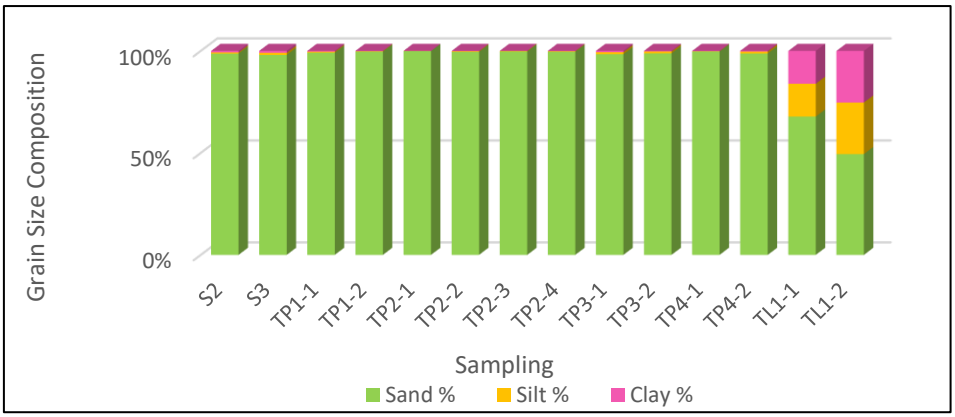

Diagram 2: Distribution of grain size composition in Usukan beach sediment.

Heavy Metal Concentration in Sediments

Table 2 shows the total concentration of heavy metals Fe, Al, and Mn in the fine-grain fraction with size <63µm. The total mean concentration and standard deviation of heavy metals determined are Al (mean 6,824±2,025 ppm), Fe (mean 17,804±6,513 ppm), and Mn (mean 300±109 ppm), and their background values are based on the average shale values (ASV) (*Turekian and Wedepohl, 1961). The heavy metal contents are also compared with the standard background limits of SQG established by NOAA (1999), also known as Screening Quick Reference Tables (SQuiRTs).

Table 2: Total concentration of heavy metals in beach sediment (fine grain size <63μm).

Samples	Heavy Metal (ppm)								
	Al			Fe			Mn		
	Min.	Mean	Max.	Min.	Mean	Max.	Min.	Mean	Max.
SP2	5,101	7,607	10,162	5,101	20,051	10,162	200	325	455
SP3	2,108	6,228	9,311	2,108	16,291	9,311	76	228	321
TP1-1	6,490	6,950	7,437	6,490	17,399	7,437	365	375	397
TP1-2	7,563	8,524	9,610	7,563	22,076	9,610	462	541	679
TP2-1	4,716	5,803	6,891	13,444	16,130	18,816	217	259	301
TP2-2	4,801	6,923	8,903	14,069	18,810	22,330	286	376	455
TP2-3	4,975	6,242	7,821	14,292	17,060	20,616	291	371	464
TP2-4	4,777	6,394	7,339	13,874	17,841	20,147	224	318	371
TP3-1	7,311	7,421	7,531	19,227	19,678	20,129	245	246	246
TP3-2	8,442	9,043	9,579	18,114	20,745	23,320	277	320	375
TP4-1	1,355	2,563	4,089	2,300	4,476	8,073	87	137	204
TP4-2	1,127	3,375	4,686	1,811	5,373	7,921	29	103	187
TL1-1	8,134	9,926	13,124	25,595	29,829	36,407	266	345	458
TL1-2	4,597	8,533	12,732	15,422	23,496	31,400	126	255	337
Mean	6,824			17,804			300		
SD +/-	2,025			6,513			109		
SQG (SQuiRTs)	4.7%			1.8%			330		
***ASV**	80,000			47,200			850		

Marine Sediment Quality Assessment

The geoaccumulation index (Igeo), contamination factor (CF), modified degree of contamination (mCd), and pollution load index (PLI) are the assessed parameters to determine the contamination level of heavy metals in the study area. The selected elements are Al, Fe, and Mn, which are the dominant elements from the parent materials and surrounding geological sources. Since there are no local background values for the study area, the average shale values (ASV) from the Earth's crust are selected as reference values for marine sediments (Turekian and Wedepohl, 1961). Table 3 shows the Igeo values (Igeo<0) that suggest no contamination for all elements (Muller, 1969). The parameters CF<1 and mCd<1.5 both suggest none to a very low degree of contamination in the study area (Hakanson, 1980). The PLI shows 0<PLI≤1, which indicates only mild pollution due to the background levels of pollutants in the marine ecosystem (Tomlinson et al., 1980). This shows that the contaminants are more likely due to natural inputs of local geology instead of anthropogenic sources.

Table 3: Sediment quality assessment based on Igeo, CF, mCd and PLI parameters.

Parameter		SP2	SP3	TP1-1	TP1-2	TP2-1	TP2-2	TP2-3	TP2-4	TP3-1	TP3-2	TP4-1	TP4-2	TL1-1	TL1-2
Igeo	Al	-3.98	-4.27	-4.11	-3.82	-4.37	-4.12	-4.26	-4.23	-4.02	-3.73	-5.55	-5.15	-3.60	-3.81
	Fe	-1.82	-2.12	-2.02	-1.68	-2.13	-1.91	-1.91	-2.05	-1.99	-1.85	-3.98	-3.72	-1.25	-1.59
	Mn	-1.97	-2.48	-1.77	-1.24	-2.30	-1.76	-1.78	-2.00	-2.38	-2.00	-3.22	-3.63	-1.89	-2.32
CF	Al	0.10	0.08	0.09	0.11	0.07	0.09	0.08	0.08	0.09	0.11	0.03	0.04	0.12	0.11
	Fe	0.42	0.35	0.37	0.47	0.34	0.40	0.40	0.36	0.38	0.42	0.09	0.11	0.63	0.50
	Mn	0.38	0.27	0.44	0.64	0.31	0.44	0.44	0.37	0.29	0.38	0.16	0.12	0.41	0.30
ΣCF		0.90	0.69	0.90	1.21	0.72	0.93	0.91	0.82	0.76	0.91	0.29	0.28	1.16	0.90
mCd		0.30	0.23	0.30	0.40	0.24	0.31	0.30	0.27	0.25	0.30	0.10	0.09	0.39	0.30
PLI		**0.25**	**0.19**	**0.24**	**0.32**	**0.20**	**0.25**	**0.24**	**0.22**	**0.22**	**0.26**	**0.08**	**0.08**	**0.32**	**0.25**

Physico-Chemical Properties Against Sediment Quality

Table 4 shows the relationship between the physico-chemical parameters (pH, MC, SOM, PSD) and the sediment quality in terms of the sum of contamination factor, modified degree of contamination, and pollution load index. From Diagram 3, it is shown that moisture content, silt, and clay composition have a positive correlation with PLI whereas pH and sand composition show a negative correlation. OM is the only geochemical parameter that shows no correlation to the PLI. Therefore, this indicates that the physico-chemical properties of sediments regulate the heavy metal content and impact the marine sediment quality.

Table 4: Relationship between the physico-chemical properties and sediment quality

Samples	Physico-Chemical Properties						Sediment Quality		
	pH	MC %	SOM %	Sand %	Silt %	Clay %	ΣCF	mCd	PLI
SP2	5.69	4.99	0.30	98.69	0.55	0.76	0.48	0.24	0.19
SP3	6.53	5.76	0.32	98.01	1.07	0.92	0.35	0.17	0.14
TP1-1	7.09	25.01	0.25	99.14	0.46	0.40	0.53	0.26	0.20
TP1-2	7.87	25.76	0.27	99.65	0.20	0.15	0.74	0.37	0.26
TP2-1	7.34	24.03	0.16	99.10	0.05	0.05	0.38	0.19	0.15
TP2-2	7.81	23.82	0.24	99.55	0.30	0.15	0.53	0.26	0.20
TP2-3	7.88	15.32	0.20	99.70	0.25	0.05	0.51	0.26	0.18
TP2-4	7.51	25.30	0.12	99.59	0.25	0.15	0.45	0.23	0.17
TP3-1	7.25	26.16	0.32	98.37	1.02	0.61	0.38	0.19	0.16
TP3-2	7.74	39.85	0.83	98.78	0.91	0.30	0.49	0.24	0.21
TP4-1	8.44	25.94	1.63	99.75	0.10	0.15	0.19	0.10	0.07
TP4-2	8.48	27.89	1.78	98.73	0.91	0.36	0.16	0.08	0.07
TL1-1	6.08	35.43	4.66	67.80	16.10	16.10	0.53	0.26	0.22
TL1-2	6.37	48.75	6.73	49.40	25.30	25.30	0.41	0.20	0.18

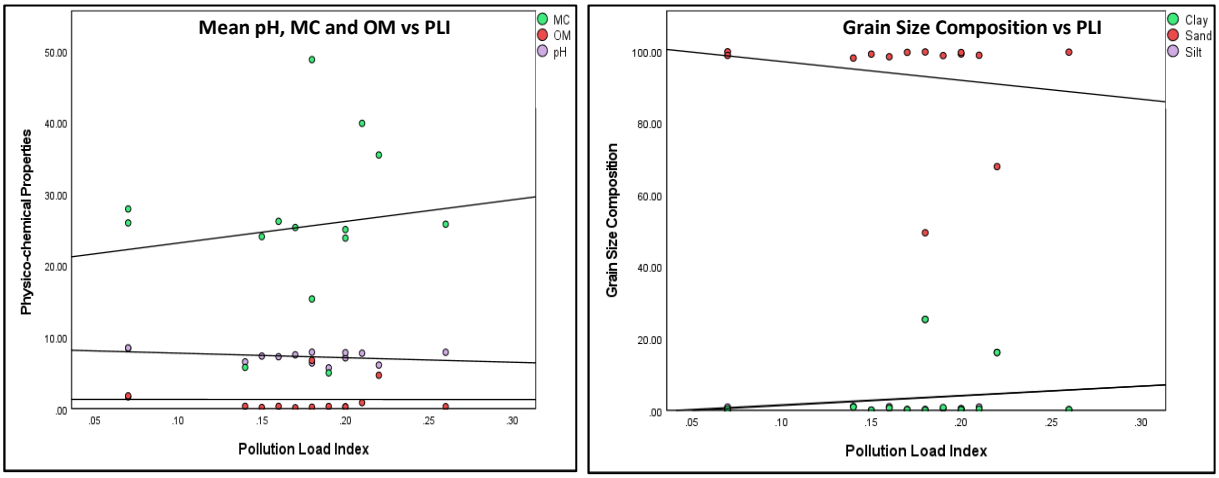

Diagram 3: Relationship between physico-chemical properties against PLI.

DISCUSSION

Physico-Chemical Properties in Marine Sediments

The sediment characteristics such as moisture content and water-holding capacity are affected by soil texture, structure, hydraulic conductivity, porosity, and permeability (Ball, 2011; Gwak and Kim, 2016). All sediments change from acidic to alkaline properties as the sampling stations are heading toward the seaward direction, probably due to the intrusion of seawater from the South China Sea, which may also impact the marine sediment quality (Ding *et al.*, 2020). Besides seawater intrusion, the dissolution of bicarbonate (HCO_3) yielded from the surrounding corals and shelled marine organisms further increased the alkaline properties of the sediments in the coastal region (Ahmed *et. al*., 2016). According to McCauley *et al*. (2017), the organic matter also affects pH values in sediments. The high SOM will release more H^+ ions into the sediments, which explains the results of Table 1. The SOM percentage also affects the moisture content. USDA (1975) also stated that sandy texture has lower SOM than clayey texture, leading to a lower buffer capacity and higher water infiltration rates in the sediments. Therefore, the fine-textured clay in mud soil has a higher affinity to hold SOM than the coarse-textured sand which contributed to the acidic properties of mud soil (Prasad and Power, 1997; Gui *et al.*, 2021). The clayey texture also influences the adsorption-desorption process of major elements such as Al in the sediments (Myung, 2008; Muli, 2017). The moisture content is inconsistent due to the difference in beach terrain, tidal cycle, storm-wave action, and evaporation or precipitation process from where the samples are collected (Scmutz and Namikas, 2018; Atherton *et al*., 2001; Namikas *et al.*, 2010). According to Luo *et al*. (2020), soil pH has the ability to control the migration and redistribution of heavy metals in the beach sediments. The negatively-charged elements, including OH- ions, can move freely in alkaline sediments and bind with other positively-charged metals such as Al, Fe and Mn from the fine-grain fraction of <63µm as shown in the ICP-OES analysis (Allaway, 1957; Sparks, 2003). Generally, the spatial distribution of heavy metals in marine sediment is also dependent on the physico-chemical properties.

Sources Identification of Heavy Metals

Heavy metals are elements with a density of more than 5 g/cm^3 (Csuros and Csuros, 2002) or with an atomic weight of at least five times greater than the water density (Tchounwoo *et al.*, 2012). Sediments are sensitive indicators when assessing heavy metals. The metals are continuously added from different inputs, either terrestrial origins (parent materials, crustal earth, atmospheric deposition, marine water column) or anthropogenic activities (industrial and agricultural activities, pesticide chemicals, domestic wastes). The accumulation of heavy metals in marine sediments that serve as a natural reservoir is thus selected for the geochemical study on heavy metal assessment (Förstner, 2006). In this study, the natural input sources of Fe and Mn elements in beach sediments are from atmospheric dust and direct volcanic origin, such as the hydrothermal fluids on the seafloor (Nicholson *et al.*, 1997; White, 2020). Although Fe is readily soluble in low oxygen levels and is essential to sustain the marine carbon cycle, it remains localized in sediments along the continental margins. The total Fe content in near-shore sediments is also high due to the high Fe^{2+}/Fe^{3+} ratio of beach sediment in aluminosilicate fractions, which were derived from the clay minerals or oxidised organic matter and accumulate in the marine sediment (Chen *et al.*, 1994; Dezileau *et al.*, 2007; Taylor and Mcquaker, 2011). The presence of Fe content in beach sediment also originated from the microbial reduction of Fe in near-shore marine sediment that formed the oxide minerals (Canfield, 1989; Grecco *et al.*, 2011). The alkaline properties also reduce the Fe solubility and restrict its mobility to build up in sediment (Lindsay, 1979; Tsai and Schmidt, 2020).

The Al content is also elevated in the sediment because it is the third most naturally occurring element in the earth's crust and from the weathering process of sedimentary rocks from both Crocker and Wariu Formation. The amphoteric properties of Al to form both organic and inorganic complexes and polymerise under a wide range of pH, temperature, dissolved substances, and long period of water exposure allows the element to exist abundantly in the marine environment (Djkstra and Fitzhugh, 2003; Amir *et al*., 2020). The alkaline properties also cause the Al element to become immobile and accumulate, which result in an elevated concentration in the sediments. The Mn element found in beach sediment along the shoreface originates from parent rocks, such as limestone and shale (Force and Cox, 1991; Govind *et al.*, 2021), cherts and basalts from the ophiolites (Sugisaki *et al.*, 1991; Narejo *et al.*, 2019). The calcareous foraminifera assemblages from the marine ecosystem also release Mn (Boyle, 1983, Bauer *et al.*, 2013; Li *et al.*, 2021). Besides Mn, the bioaccumulation of aquatic organisms is also enriched in Al in the seawater column, which ultimately also deposits in sediment (Moore and Bostrom, 1978; Neff, 2002). Other anthropogenic activities that may influence sediment quality are crop fertilization, pesticide chemicals, and other domestic or industrial wastes. In conclusion, the primary contributing factors for the heavy metal content in the sediments are natural sources such as the oceanographic setting, parent rock materials, and local geology. All the heavy metal burdens are transported from higher regions and accumulate in Usukan coastal beach that serves as a natural sink.

Marine Sediment Quality Assessment and Correlation

The Pollution Load Index (PLI) is a standardized system to assess the degree to which the sediment is associated with heavy metals and detect the pollution levels in sediments. The PLI values show very low pollution primarily due to the background level of pollutants in the study area. When The Quality

compared with the background ASV, the average concentration of Al (6,824±2,025 ppm), Fe (17,804±6,513 ppm), and Mn (300±109 ppm) metals are within the permissible background levels of 80,000 ppm, 47,200 ppm, and 850 ppm, respectively (Turekian and Wedepohl, 1961). The heavy metal concentrations are also below the standard limits established in the SQuiRTs for marine sediments (NOAA, 1999), which further justifies that the minor deterioration of pollutants in the study area is more likely from natural inputs than anthropogenic sources. The accumulation of metal pollutants in sediment loads are also greatly influenced by the fine granulometric fraction as the fine texture has greater pollutant retention and metal adsorption due to a higher specific surface area to volume ratio than the sand fraction (Abolfazl and Ahmad, 2012; Maher *et al*., 1999; Hart, 1982; Durães *et al.,* 2018).

On the contrary, the sand fraction is coarser and has lower water retention but higher drainage, hence indicating a negative correlation with the metal pollutants in PLI. The slight negative correlation between pH against PLI also suggests that soil acidity increases the leaching of heavy metals to accumulate in sediments and affects the quality of marine sediment (Zhang *et al.,* 2018). Overall, the sediment quality assessment does not show any significant impacts of metal pollution or severe threat to aquatic organisms and human health in the Usukan coastal beach.

CONCLUSION

The geochemical and statistical assessment of heavy metals indicates a very minimal degree of pollution in the marine sediments. The sediment quality indices show that the heavy metal contents of Al (6,824ppm), Fe (17,804ppm), and Mn (300ppm) are within the background values and standard limits of the Sediment Quality Guideline for marine sediments. The pollution load index is influenced by the physico-chemical properties of sediments such as the acidic to alkaline properties (pH 5.69-8.48), low to moderate moisture content (4.99-39.85%), very low to moderately high organic matter (0.12-6.73%) and fine to coarse texture which control the distribution of heavy metals to various parts of the marine sediments. The background pollutants are mainly from the geological source rocks comprising sedimentary rocks from Crocker Formation and limestone, shale, and ophiolitic rocks from Wariu Formations that are transported by rivers, leachate, or run-offs to the marine sediments near the coastal regions. In short, the geochemical and statistical assessment implied that there are no significant impacts of metal pollution or severe threat to the marine sediment quality in Usukan coastal beach. Nevertheless, further investigations and ongoing monitoring are highly recommended to assess the long-term effects of their inputs into the Kota Belud marine ecosystem.

ACKNOWLEDGEMENT

We would like to express our heartfelt thanks to Universiti Malaysia Sabah for providing the laboratory facilities at the Faculty of Science and Natural Resources and financial support using external research funding from MOSTI with Code TR@M001-2019.

REFERENCES

Abolfazl, N. & Ahmad, I. 2012. Sediment quality assessment of Klang Estuary, Malaysia. Aquatic Ecosystem Health & Management: 15(3): 287-293.

Ahmed, A. & Askri, B. 2016. Seawater Intrusion Impacts on the Water Quality of the Groundwater on the Northwest Coast of Oman. Water Environment Research: 88: 732-740.

Allaway, W.H. 1957. pH, soil acidity and plant growth. Soil: 67-71.

Amir, M., Iqbal, M., Zainal, S. & Manap, A. 2020. Static Adsorption of Amphoteric Surfactant. Offshore Technology Conference.

Atherton, R.J., Baird, A.J. & Wiggs, G.F.S. 2001. Intertidal dynamics of surface moisture content on a meso-tidal beach. J. Coastal Res.: 17: 482–489.

Ball, J. 2001. Soil and Water Relationships. Noble Research Institute, 1 Sep 2001, Retrieved: https://www.noble.org/news/publications/ag-news-and-views/2001/september/soil-and-water-relationSSships/.

Bauer, A., Radziejewska, T., Liang, K., Kowalski, N., ... & Waniek, J.J. 2013. Regional differences of hydrographical and sedimentological properties in the Beibu Gulf, South China Sea. Journal of Coastal Research: 66 (10066): 49-71.

Birch, G. 2018. A review of chemical-based sediment quality assessment methodologies for the marine environment. Marine pollution bulletin: 133: 218-232.

Boyle, E.A. 1983. Manganese carbonate overgrowths on foraminifera tests. Geochimica et Cosmochimica Acta: 47(10).

BSI. 1990. BS1377: 1990 British Standard Methods of Tests for Soils for Civil Engineering Purposes. London: British Standard Institution (BSI).

Canfield, D. 1989. Reactive iron in marine sediments. Geochimica et cosmochimica acta.: 53: 619-32.

Chen, S., Takematsu, N., Ambe, S., Ament, A. & Ambe, F. 1994. A Mössbauer spectroscopy study on iron in marine sediments. Hyperfine Interactions: 91: 759-763.

Chuan, O.M. & Yunus, K. 2019. Sediment and organisms as marker for metal pollution. In Monitoring of Marine Pollution. IntechOpen: 1-19.

Clement, J.F. & Keij, J. 1958. Geology of the Kudat Peninsula, North Borneo (Compilation) GR783. Unpublished Reports of the Royal Dutch Shell Group of Companies in British Borneo.

Csuros, M. & Csuros, C. 2002. Environmental Sampling and Analysis for Metals. Boca Raton, USA: Lewis Publishers.

Collenette, P. 1957. Notes on the geology of the headwaters of the Labuk, Sugut and Karamuak Rivers. Brit. Borneo Geol. Suv. Ann. Rep.:153-162.

Dezileau, L. & Pizarro, C. & Rubio, M. 2007. Sequential extraction of iron in marine sediments from the Chilean continental margin. Marine Geology - MAR GEOLOGY: 241: 111-116.

Ding, Z., Koriem, M.A., Ibrahim, S.M., Antar, A.S., Ewis, M.A., He, Z. & Kheir, A. M. 2020. Seawater intrusion impacts on groundwater and soil quality in the northern part of the Nile Delta, Egypt. Environmental Earth Sciences: 79(13): 1-11.

Djkstra, F. & Fitzhugh, R. 2003. Aluminum solubility and mobility in relation to organic carbon in surface soils affected by six tree species of the North Eastern United States. Geoderma: 114: 33-47.

Durães, N., Novo, L.A., Candeias, C. & Da Silva, E.F. 2018. Distribution, transport and fate of pollutants. In Soil pollution. Academic Press: 29-57.

Force, E.R. & Cox, L.J. 1991. Manganese contents of some sedimentary rocks of Paleozoic age in Virginia. US Government Printing Office.

Förstner, U. 2006. Contaminated sediments: lectures on environmental aspects of particle-associated chemicals in aquatic systems. Chicago: The University of Chicago Press Vol. 21.

Gopal, V., Achyuthan, H. & Jayaprakash, M. 2017. Assessment of trace elements in Yercaud Lake sediments, southern India. Environ Earth Sci.: 76: 63.

Govind, A.V., Behera, K., Dash, J.K., Balakrishnan, S., Bhutani, R., Managave, S. & Srinivasan, R. 2021. Trace element and isotope Geochemistry of Neoarchean carbonate rocks from the Dharwar craton, southern India: Implications for depositional environments and mantle influence on ocean chemistry. Precambrian Research: 357.

Grecco, L., Gómez, E., Botté, S., Marcos, Á., Marcovecchio, J. & Cuadrado, D. 2011. Natural and anthropogenic heavy metals in estuarine cohesive sediments: Geochemistry and bioavailability. Ocean Dynamics - OCEAN DYN: 61: 285-293.

Gui, Y., Zhang, Q., Qin, X. & Wang, J. 2021. Influence of Organic Matter Content on Engineering Properties of Clays. Advances in Civil Engineering 2021: 1-11.

Gwak, Y.S. & Kim, S.H. 2016. Factors Affecting Soil Moisture Spatial Variability for a Humid Forest Hillslope. Hydrological Processes.

Hakanson, L. 1980. Ecological risk index for aquatic pollution control. A sedimentological approach. Water. Res.: 14: 975–1001.

Hall, R. & Breitfeld, H.T. 2017. Nature and Demise of the Proto-South China Sea. Bulletin of the Geological Society of Malaysia: 63.

Han, F.X., Kingery, W.L. & Selim, H.M. 2001. Accumulation, redistribution, transport, and bioavailability of heavy metals in waste-amended soils. CRC Press: In Trace Elements in Soil: 161-190.

Hart, B.T. 1982. Uptake of trace metals by sediments and suspended particulates: A review. Hydrobiol.: 91: 299–313.

Jayamurali, D., Varier, K., Liu, W., Jegadeesh, P.H., Yaacov, B.D., Shen, X. & Gajendran, B. 2021. An Overview of Heavy Metal Toxicity. ReseachGate.

Junaidi, A. & Basir, J. 2012. Aptian to Turonian radiolaria from the Darvel Bay Ophiolite Complex, Kunak, Sabah. Bulletin of Geol. Soc. Malaysia: 58: 89-96.

Le Pera, E., Arribas, J., Critelli, S. & Tortosa, A. 2001. The effects of source rocks and chemical weathering on the petrogenesis of siliciclastic sand from the Neto River (Calabria, Italy): implications for provenance studies. Sedimentology: 48(2): 357-378.

Li, N., Feng, D., Wan, S., Peckmann, J., Guan, H., Wang, X., ... & Chen, D. 2021. Impact of methane seepage dynamics on the abundance of benthic foraminifera in gas hydrate bearing sediments: New insights from the South China Sea. Ore Geology Reviews: 104247.

Li, C., Zhou, K., Qin, W., Tian, C., Qi, M., Yan, X. & Han, W. 2019. A review on heavy metals contamination in soil: effects, sources, and remediation techniques. Soil and Sediment Contamination: An International Journal: 28(4): 380-394.

Lindsay, W.L. 1979. Chemical equilibria in soils. New York: John Wiley & Sons.

Luo, J.Z., Sheng, B.X. & Sheng, Q.Q. 2020. A review on the migration and transformation of heavy metals influence by alkali/alkaline earth metals during combustion. Journal of Fuel Chemistry and Technology: 48 (11).

Maher, W., Batkey, G.E. & Lawrence, I. 1999. Assessing the health of sediment ecosystems: Use of chemical measurements. Freshwater Biol.: 41: 361–372.

McCauley, A., Jones, C. & Olson-Rutz, K. 2017. Soil pH and Organic Matter. Nutrient Management: 8: 1-4.

Moore, C. & Bostrom, K. 1978. The elemental compositions of lower marine organisms. Chemical Geology - CHEM GEOL: 23: 1-9.

Muli, M. M. 2017. Metals in Plants and Soils Along a Section of Nairobi. School of Pure and Applied Science, Kenyatta University.

Müller, G. 1969. Index of geoaccumulation in the sediments of the Rhine River. Geojournal: 2:108–118.

Myung, C. J. 2008. Heavy Metal Concentrations in Soils and Factors Affecting Metal Uptake by Plants in the Vicinity of a Korean Cu-W Mine. US National Library of Medicine: 8(4): 2413-2423.

Namikas, S.L., Edwards, B.L., Bitton, M.C.A., Booth, J.L. & Zhu, Y. 2010. Temporal and spatial variability in the surface moisture content of a fine-grained beach. Geomorphology: 114: 303–310.

Narejo, A.A., Shar, A.M., Fatima, N. & Sohail, K. 2019. Geochemistry and origin of Mn deposits in the Bela ophiolite complex, Balochistan, Pakistan. Journal of Petroleum Exploration and Production Technology: 9(4): 2543-2554.

Neff, J. M. 2002. Bioaccumulation in Marine Organisms. Massachusetts. Elsevier Publisher: 175-189.

Nicholson, K., Hein, J.R., Biilm, B. & Dasgupta, S. 1997. Manganese Mineralization: Geochemistry and Mineralogy of Terrestrial and Marine Deposits. Geological Society of London Special Publication: 119: 370.

NOAA, U. 1999. Screening Quick Reference Tables (SQuiRTs). Coastal protection and restoration

division. National Marine Fisheries Service (NMFS). US Dep. Commer. National Oceanic

and Atmospheric Adminstration (NOAA) Tech. Memo.: Our Living Oceans. Report on the status of US living marine resources, 1999.

Prasad, R. and J.F. Power. 1997. Soil Fertility Management for Sustainable Agriculture. New York: Lewis Publishers.

Sanudin, T. & Baba, M. 2007. Pengenalan kepada Stratigrafi. Kota Kinabalu: Penerbit Universiti Malaysia Sabah.

Seaward, M.R.D. & Richardson, D.H.S. 1989. Atmospheric sources of metal pollution and effects on vegetation. Heavy metal tolerance in plants: Evolutionary aspects: 75-92.

Schmutz, P. & Namikas, S. 2018. Measurement and modeling of the spatiotemporal dynamics of beach surface moisture content. Aeolian Research: 34: 35–48.

Sparks, D.L. 2003. Environmental soil chemistry. London: Elsevier, Academic Press.

Sugisaki, R., Sugitani, K. & Adachi, M. 1991. Manganese carbonate bands as an indicator of hemipelagic sedimentary environments. The Journal of Geology: 99(1): 23-40.

Taylor, K.G. & Macquaker, J.H. 2011. Iron minerals in marine sediments record chemical environments. Elements: *7*(2): 113-118.

Tchounwou, P.B., Yedjou, C.G., Patlolla, A.K. & Sutton DJ. 2012. Heavy metal toxicity and the environment. Exp Suppl.: 101:133-64.

Tomlinson, D.L., Wilson, J.G., Harris, C.R. & Jeffrey, D.W. 1980. Problems in the assessment of heavy-metal levels in estuaries and the formation of a pollution index. Helgoländer meeresuntersuchungen: 33(1-4), 566-575.

Tongkul, F. 2006. The structural style of Lower Miocene Sedimentary Rocks, Kudat Peninsula, Sabah. Bulletin of the Geol. Soc. of Malaysia: 49: 119-124.

Tsai, H.H. & Schmidt, W. 2020. pH-dependent transcriptional profile changes in iron-deficient Arabidopsis roots. BMC Genomics: 21: 694.

Turekian, K.K. & Wedepohl, K.H. 1961. Distribution of the elements in some major units of the earth's crust. Geol Soc Am Bull.: 72(2): 175-92.

United States Department of Agriculture, Soil Conservation Service (USDA). 1975. Soil Taxonomy: A Basic System of Soil Classification for Making and Interpreting Soil Surveys. Soil Surv. Staff. U.S. Dep. Agric. Handbook: 436.

U.S. Environmental Protection Agency. 2014. Method 6010D (Revision 4): Inductively coupled-plasma atomic emission spectrometry. Washington, DC: Environmental Protection Agency.

Vallius, H., Ryabchuk, D. & Kotilainen, A. 2007. Distribution of heavy metals and arsenic in soft surface sediments of the coastal area off Kotka, northeastern Gulf of Finland, Baltic Sea. Geological Survey of Finland Special Paper: 45: 33–48.

Xiang, M., Li, Y., Yang, J., Lei, K., Li, Y., Li, F., Zheng, D., Fang, X. & Cao, Y. 2021. Heavy metal contamination risk assessment and correlation analysis of heavy metal contents in soil and crops. Environmental Pollution: 278.

Yang, W., Cao, Z., Zhang, H. & Lang, Y. 2021. A national wide evaluation of heavy metals pollution in surface sediments from different marginal seas along China Mainland, Regional Studies in Marine Science: 42.

White, W.M. 2020. Geochemistry: The Oceans as a Chemical System. Oxford: John Wiley & Sons.

Wuana, R. & Okieimen, F. 2011. Heavy Metals in Contaminated Soils: A Review of Sources, Chemistry, Risks and Best Available Strategies for Remediation. ResearchGate: ISRN Ecology 2011.

Zhang, X., Zhong, T., Liu, L. & Ouyang, X. 2015. Impact of Soil Heavy Metal Pollution on Food Safety in China. PLoS ONE: 10(8).

Zhang, Y., Zhang, H., Zhang, Z., Liu, C., Sun, C., Zhang, W. & Marhaba, T. 2018. pH effect on heavy metal release from a polluted sediment. Journal of Chemistry.